Cell Reports

Article

An anaphase surveillance mechanism prevents micronuclei formation from frequent chromosome segregation errors

Graphical abstract

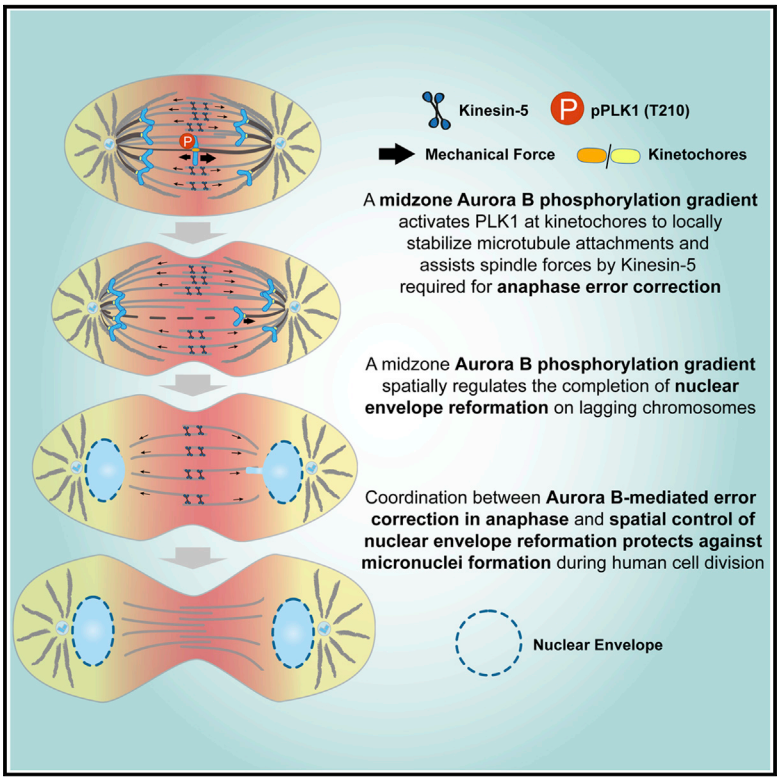

Highlights

- Anaphase lagging chromosomes are frequent but rarely form micronuclei
- A midzone Aurora B activity gradient prevents micronuclei from segregation errors
- Midzone Aurora B assists spindle forces at the kinetochores to correct errors
- Aurora B spatially regulates nuclear envelope reformation on lagging chromosomes

Authors

Bernardo Orr, Filipe De Sousa, Ana Margarida Gomes, Olga Afonso, Luísa T. Ferreira, Ana C. Figueiredo, Helder Maiato

Correspondence

maiato@i3s.up.pt

In brief

Orr et al. show that a spindle midzone-based Aurora B phosphorylation gradient mediates a surveillance mechanism that prevents micronuclei formation from frequent chromosome segregation errors by integrating error correction during anaphase with spatial control of nuclear envelope reassembly on lagging chromosomes in human cells.

Orr et al., 2021, Cell Reports *37*, 109783
November 9, 2021
https://doi.org/10.1016/j.celrep.2021.109783

CellPress

Cell Reports

CellPress
OPEN ACCESS

Article

An anaphase surveillance mechanism prevents micronuclei formation from frequent chromosome segregation errors

Bernardo Orr,[1,2] Filipe De Sousa,[1,2,4] Ana Margarida Gomes,[1,2] Olga Afonso,[1,2,5] Luísa T. Ferreira,[1,2] Ana C. Figueiredo,[1,2] and Helder Maiato[1,2,3,6,*]

[1]Chromosome Instability & Dynamics Group, i3S - Instituto de Investigação e Inovação em Saúde, Universidade do Porto, Rua Alfredo Allen 208, 4200-135 Porto, Portugal

[2]Instituto de Biologia Molecular e Celular, Universidade do Porto, Rua Alfredo Allen 208, 4200-135 Porto, Portugal

[3]Cell Division Group, Department of Biomedicine, Faculdade de Medicina, Universidade do Porto, Alameda Prof. Hernâni Monteiro, 4200-319 Porto, Portugal

[4]Present address: Radiation Oncology Division, Geneva University Hospitals (HUG), Avenue de la Roseraie 53, 1205 Geneva, Switzerland

[5]Present address: Department of Biochemistry, Sciences II, University of Geneva, Quai Ernest-Ansermet 30, 1211 Geneva, Switzerland

[6]Lead contact

*Correspondence: maiato@i3s.up.pt

https://doi.org/10.1016/j.celrep.2021.109783

SUMMARY

Micronuclei are a hallmark of cancer and several other human disorders. Recently, micronuclei were implicated in chromothripsis, a series of massive genomic rearrangements that may drive tumor evolution and progression. Here, we show that Aurora B kinase mediates a surveillance mechanism that integrates error correction during anaphase with spatial control of nuclear envelope reassembly to prevent micronuclei formation. Using high-resolution live-cell imaging of human cancer and non-cancer cells, we uncover that anaphase lagging chromosomes are more frequent than previously anticipated, yet they rarely form micronuclei. Micronuclei formation from anaphase lagging chromosomes is prevented by a midzone-based Aurora B phosphorylation gradient that stabilizes kinetochore-microtubule attachments and assists spindle forces required for anaphase error correction while delaying nuclear envelope reassembly on lagging chromosomes, independently of microtubule density. We propose that a midzone-based Aurora B phosphorylation gradient actively monitors and corrects frequent chromosome segregation errors to prevent micronuclei formation during human cell division.

INTRODUCTION

Micronuclei (MN) are small-sized nuclei derived from whole chromosomes or chromosome fragments that fail to incorporate into daughter nuclei during cell division (Guo et al., 2019). MN formation is widely used as a biomarker of cancer and inflammation, as well as several metabolic, reproductive, cardiovascular, and neurodegenerative disorders (Fenech et al., 2020). Recently, MN have drawn exceptional attention due to their causal link with chromothripsis, a series of massive genomic rearrangements that may drive rapid tumor evolution and account for acquired drug resistance and oncogene activation (Crasta et al., 2012; Ly and Cleveland, 2017; Shoshani et al., 2021; Stephens et al., 2011; Zhang et al., 2015). Chromosome segregation errors underlying MN formation are normally prevented before anaphase by a tension-dependent correction mechanism involving the chromosomal passenger complex (CPC) protein Aurora B kinase at centromeres (Lampson and Grishchuk, 2017), under surveillance of the spindle assembly checkpoint (SAC) that monitors the formation of kinetochore-microtubule (KT-MT) attachments (Musacchio, 2015). Despite this, between 0.1% and 10% of human primary and non-transformed or chromosomally stable cancer cells progress into anaphase with one or few chromosomes lagging behind due to merotelic attachments (Bakhoum et al., 2014; Cimini et al., 2002; Thompson and Compton, 2011; Worrall et al., 2018). Merotelic attachments, in which a single KT is attached to MTs from both spindle poles (Cimini et al., 2001), evade SAC detection, and the resulting anaphase lagging chromosomes may lead to MN formation (Crasta et al., 2012). However, whether anaphase lagging chromosomes inevitably result in MN remains controversial, with frequencies ranging from 18% to 78% reported in the literature (Cohen-Sharir et al., 2021; Fonseca et al., 2019; Huang et al., 2012; Thompson and Compton, 2011; Worrall et al., 2018). Importantly, despite the fact that chromosomal instability (CIN) is a hallmark of human cancers (Bakhoum and Cantley, 2018; Hanahan and Weinberg, 2000), MN prevalence in both cancer and non-cancer cells is relatively infrequent (typically less than 5%–10% of the cells; Bonassi et al., 2011; Jdey et al., 2017), even after induction of massive chromosome segregation errors by experimental abrogation of the SAC (Cohen-Sharir et al., 2021), implying the existence of surveillance

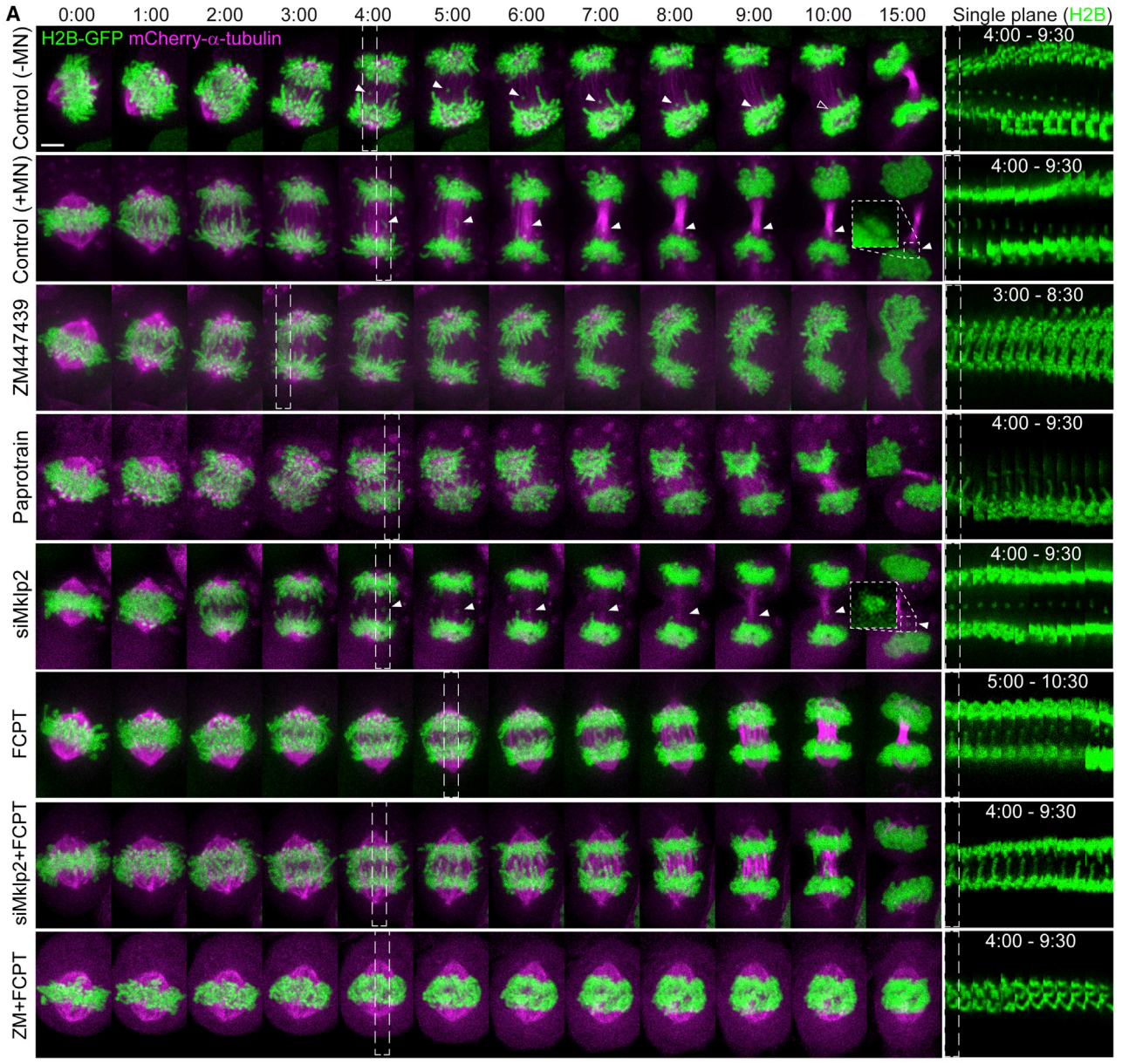

B

	Dividing cells with micronuclei (%)		Lagging chromosomes that formed micronuclei (%)	
	U2OS	RPE1	U2OS	RPE1
Control	11 (n=198)	2 (n=134)	9 (n=169)	6 (n=16)
siMklp2	28 (n=43)	11 (n=27)	17 (n=58)	25 (n=12)

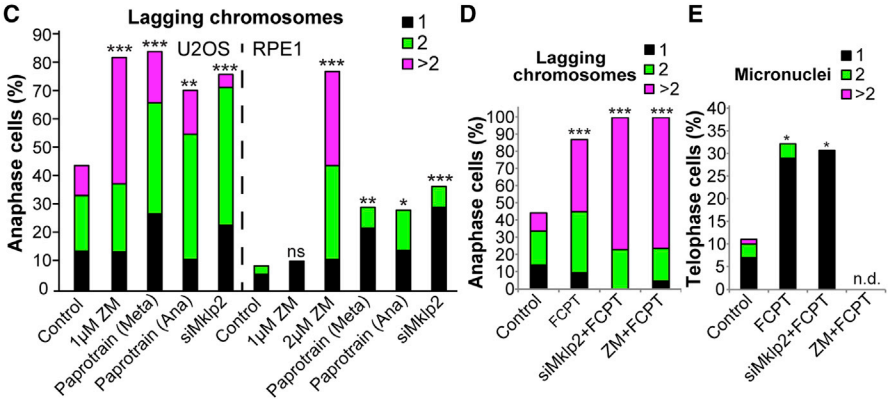

(legend on next page)

mechanisms that either prevent MN formation from SAC-invisible mitotic errors or account for the clearance of micronucleated cells. Clearance of micronucleated cells involves an innate immune response mediated by cGAS-STING, which is thought to sense cytosolic DNA on MN with ruptured nuclear envelopes (NEs) (Mackenzie et al., 2017; Santaguida et al., 2017), and a p53-dependent mechanism that causes cell cycle arrest and apoptosis (Fonseca et al., 2019; Janssen et al., 2011; Sablina et al., 1998; Thompson and Compton, 2010). Whether cells also have mechanisms that prevent MN formation from chromosome segregation errors that evade SAC surveillance remains unknown. Given their potential role in the genesis of MN and the strong implications for human health, here, we investigated how human cells deal with SAC-invisible mitotic errors that result in anaphase lagging chromosomes. Our findings uncover an active surveillance mechanism operating during anaphase that protects against MN formation from frequent chromosome segregation errors during human cell division.

RESULTS

Anaphase errors are frequent but rarely result in MN

Many intrinsic factors influence whether a lagging chromosome will result in a MN, depending on the chromosome (Worrall et al., 2018), the delay and position relative to the main segregating chromosome mass (Fonseca et al., 2019), or the presence or absence of centromeres (Norppa and Falck, 2003). In addition, external factors, such as the spatiotemporal resolution of the microscopy setup and sample size, may undermine our capacity to accurately determine the fate of lagging chromosomes in living cells. To mitigate these external limitations, we used 4D live-cell spinning-disk confocal microscopy covering the entire chromosome set and the mitotic spindle, with 30-s temporal resolution, to determine the fate of anaphase lagging chromosomes in human cells. This allowed the unequivocal identification of all lagging chromosomes, including those of highly transient nature that normally resolve early in anaphase. We found that 9% of chromosomally stable (non-transformed) RPE1 cells and 44% of chromosomally unstable (transformed) U2OS cells displayed at least one transient lagging chromosome during anaphase (Figures 1A, 1C, and S1A; Videos S1 and S2). However, only 6% and 9% of the lagging chromosomes in RPE1 and U2OS cells, respectively, resulted in MN (Figures 1A, 1B, and S1A; Videos S1 and S2). Thus, most lagging chromosomes in both transformed and non-transformed human cells are corrected during anaphase and show a strong bias to re-integrate the main nuclei.

Anaphase errors are normally corrected by a mechanism relying on a midzone-based Aurora B phosphorylation gradient

In anaphase, Aurora B transfers from centromeres to the spindle midzone, where it forms a phosphorylation gradient (Afonso et al., 2014; Fuller et al., 2008). To investigate whether Aurora B plays a role in anaphase error correction, we performed acute inhibition of Aurora B activity immediately after anaphase onset with 1 to 2 μM ZM447439, a concentration range that did not compromise Aurora A activity (Figures 1A, 1C, 2A, 2B, S1A, and S2A; Videos S1, S2, and S3). In parallel, we inhibited Aurora B transport to the spindle midzone either by acute inhibition of Mklp2/kinesin-6 immediately after anaphase onset with paprotrain (Tcherniuk et al., 2010) or constitutive Mklp2 depletion by RNAi (Gruneberg et al., 2004; Figures 1A, 1C, 2A, 2B, S1A, S2B–S2E, and S3A–S3D; Videos S1, S2, and S3). Although ZM447439 treatment did not affect the re-localization of Aurora B to the spindle midzone (normally occurring within the first 2 min after anaphase onset), this was significantly delayed or abolished after paprotrain treatment or Mklp2 knockdown, respectively (Figures 2A and 2B; Video S3). All conditions abolished the formation of a phosphorylation gradient on both segregating and lagging chromosomes (Figures S4A–S4C) while significantly increasing the frequency of anaphase cells with lagging chromosomes, as well as the number of lagging chromosomes per cell in both RPE1 and U2OS cells (Figures 1A, 1C, and S1A; Videos S1 and S2). Noteworthy, resolution of anaphase chromosome bridges depended on Aurora B activity, but not on its midzone localization (Figure S1B). Thus, anaphase lagging chromosomes are more frequent than previously anticipated, becoming particularly evident after inhibition of a midzone-based Aurora B phosphorylation gradient, suggesting that Aurora B mediates an active error correction mechanism operating during anaphase.

A midzone-based Aurora B phosphorylation gradient prevents MN formation from anaphase lagging chromosomes

Next, we determined whether a midzone-based Aurora B phosphorylation gradient prevents MN formation from anaphase lagging chromosomes. Global inhibition of Aurora B activity in anaphase impacted chromosome separation by affecting

Figure 1. Anaphase lagging chromosomes are frequent but normally corrected by a midzone-based Aurora B phosphorylation gradient that assists spindle forces to prevent micronuclei formation

(A) U2OS cells stably expressing H2B-GFP (H2B) and mCherry-α-tubulin under specified conditions. White dashed rectangular regions of interest (ROIs) indicate the first frame shown in the single-plane kymographs on the right for each condition. White arrowheads track lagging chromosomes until their eventual re-integration in the main nuclei or form MN. Higher magnification (3×) insets show single-channel (H2B) examples of MN. Scale bar represents 5 μm.

(B) Frequency of micronuclei formation and lagging chromosomes that result in micronuclei in U2OS and RPE1 cells, with and without Mklp2. The total number of cells and chromosomes analyzed is indicated between parentheses for each condition.

(C) Frequency of U2OS and RPE1 cells with anaphase lagging chromosomes under the specified conditions. U2OS cells: control n = 198; 1 μM ZM447439 (ZM) n = 29; 10 μM paprotrain added in metaphase (Meta) n = 33; 10 μM paprotrain added in anaphase (Ana) n = 45; siMklp2 n = 43; analyzed using Fisher's exact two-tailed test. RPE1 cells: control n = 136; 1 μM ZM447439 (ZM) n = 19; 2 μM ZM447439 (ZM) n = 18; 10 μM paprotrain added in metaphase (Meta) n = 27; 10 μM paprotrain added in anaphase (Ana) n = 21; siMklp2 n = 27.

(D and E) Frequency of U2OS cells with (D) lagging chromosomes and (E) MN for the specified conditions (control n = 198, 100 μM FCPT n = 31, siMklp2 + 100 μM FCPT n = 13, 100 μM FCPT + 1 μM ZM n = 21; analyzed using Fisher's exact two-tailed test).

All data were pooled from at least 3 independent experiments. n.d., not determined; *$p \leq 0.05$, **$p \leq 0.01$, and ***$p \leq 0.001$. See also Figures S1, S2, and S5.

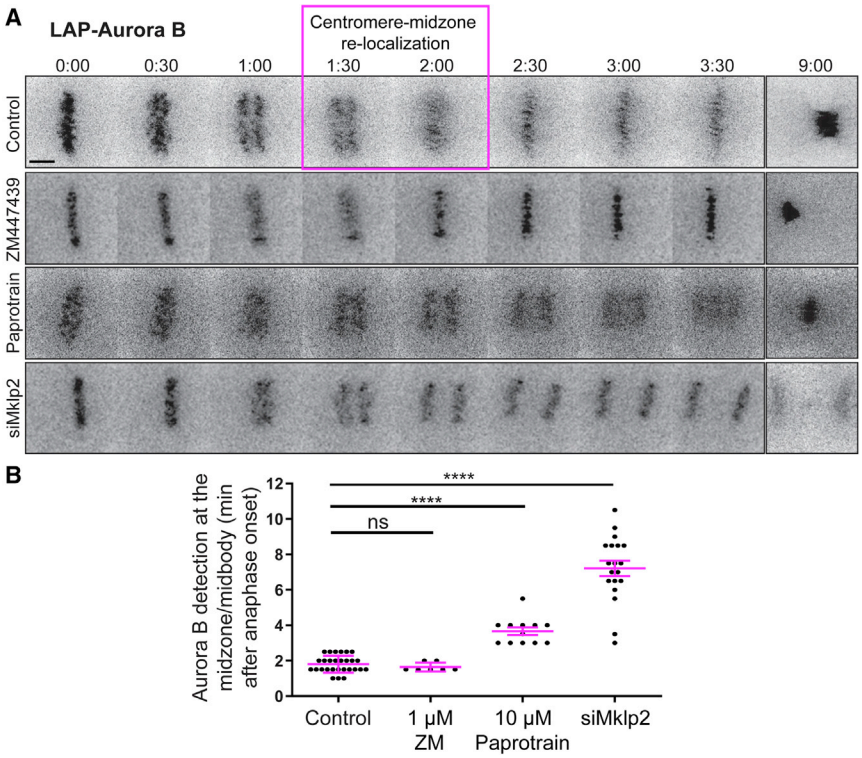

Figure 2. Mklp2 is required for dynamic Aurora B re-localization from centromeres to the spindle midzone

(A) Selected time frames of representative HeLa cells stably expressing LAP-Aurora B in control, 1 μM ZM447439 (ZM) treated, 10 μM paprotrain (Papro) treated, or after depletion of Mklp2. Time, min:s. ZM and paprotrain treatments were added within the 1st min of anaphase onset. Magenta box highlights the narrow time window of centromere to midzone re-localization in control cells. Scale bar represents 5 μm.

(B) Quantification of the time it takes to detect Aurora B at the midzone or midbody after anaphase onset (control n = 28, ZM n = 7, paprotrain n = 14, siMklp2 n = 19; data were pooled from at least 3 independent experiments, analyzed using a two-tailed t test; error bars indicate mean ± SD; n.s., non-significant; ****$p \leq 0.0001$).

See also Figures S3 and S4.

spindle midzone organization and elongation, as well as chromosome segregation distance (Figures 1A and S5A–S5C). We also observed a massive increase in the frequency of chromosome bridges, which, upon decondensation, often resulted in the formation of a continuous chromatin mass with the other partially segregated chromosomes (Figures 1A and S1B; Videos S1 and S2). Paprotrain treatment after anaphase onset delayed but did not fully prevent Aurora B localization at the spindle midzone, yet it strongly reduced spindle elongation velocity (Figures 2A, 2B, and S5B). Importantly, the frequency of cells with lagging chromosomes that resulted from acute paprotrain treatment in metaphase or anaphase were indistinguishable from the one observed after constitutive Mklp2 depletion (Figure 1C), suggesting an anaphase-specific role for a midzone-based Aurora B phosphorylation gradient in error correction. Therefore, we concentrated on investigating MN formation from mitotic errors after Mklp2 depletion. The frequency of telophase cells with MN increased approximately 3- and 5-fold in U2OS and RPE1 cells, respectively (Figure 1B). Moreover, the probability of lagging chromosomes resulting in MN also proportionally increased in both cell types (Figure 1B). Thus, a midzone-based Aurora B phosphorylation gradient is required to prevent MN formation from frequent chromosome segregation errors.

Midzone Aurora B mediates anaphase error correction by assisting the mechanical transduction of spindle forces at the KT-MT interface

Lagging chromosomes may be corrected during anaphase by the mechanical action of spindle forces that ultimately resolve merotelic attachments (Cimini et al., 2003, 2004; Courtheoux et al., 2009). However, the underlying molecular mechanism remained unclear. In yeast, spindle elongation relies on the functional interaction between the CPC and kinesin-5 (Rozelle et al., 2011). To investigate whether Aurora B mediates anaphase error correction by regulating spindle forces at the KT-MT interface, we attenuated spindle elongation in U2OS cells with FCPT, which prevents interpolar MT sliding by locking kinesin-5 on MTs (Collins et al., 2014), and compared its effects with those observed after the disruption of Aurora B function in anaphase. Acute FCPT treatment at anaphase onset strongly impaired spindle elongation, chromosome separation velocity, and chromosome segregation distance (Figures 1A, 1D, and S5A–S5C; Video S1). A similar effect was observed after acute Aurora B inhibition at anaphase onset, but not after acute Mklp2 inhibition with paprotrain (also at anaphase onset) or its constitutive depletion by RNAi (Figures 1A and S5A–S5C; Video S1). Combination of FCPT treatment with acute Aurora B inhibition at anaphase onset or Mklp2 depletion did not impair spindle elongation and chromosome separation beyond the effect caused by FCPT treatment alone (Figures 1A and S5A–S5C; Video S1). In agreement, we observed an equivalent increase in the frequency of anaphase cells with lagging chromosomes and a consequent increase in telophase cells with MN, either with FCPT alone or combined with acute Aurora B inhibition or Mklp2 depletion, in line with our previous observations after Aurora B inhibition or Mklp2 depletion alone (Figures 1A–1E; Video S1). These data suggest that anaphase error correction is mediated by a midzone-based Aurora B phosphorylation gradient that assists the mechanical transduction of spindle forces at the KT-MT interface.

A midzone-based Aurora B phosphorylation gradient locally stabilizes KT-MT attachments required for anaphase error correction and MN prevention

To investigate whether anaphase error correction requires the establishment of stable KT-MT attachments, we performed a

CellPress
OPEN ACCESS

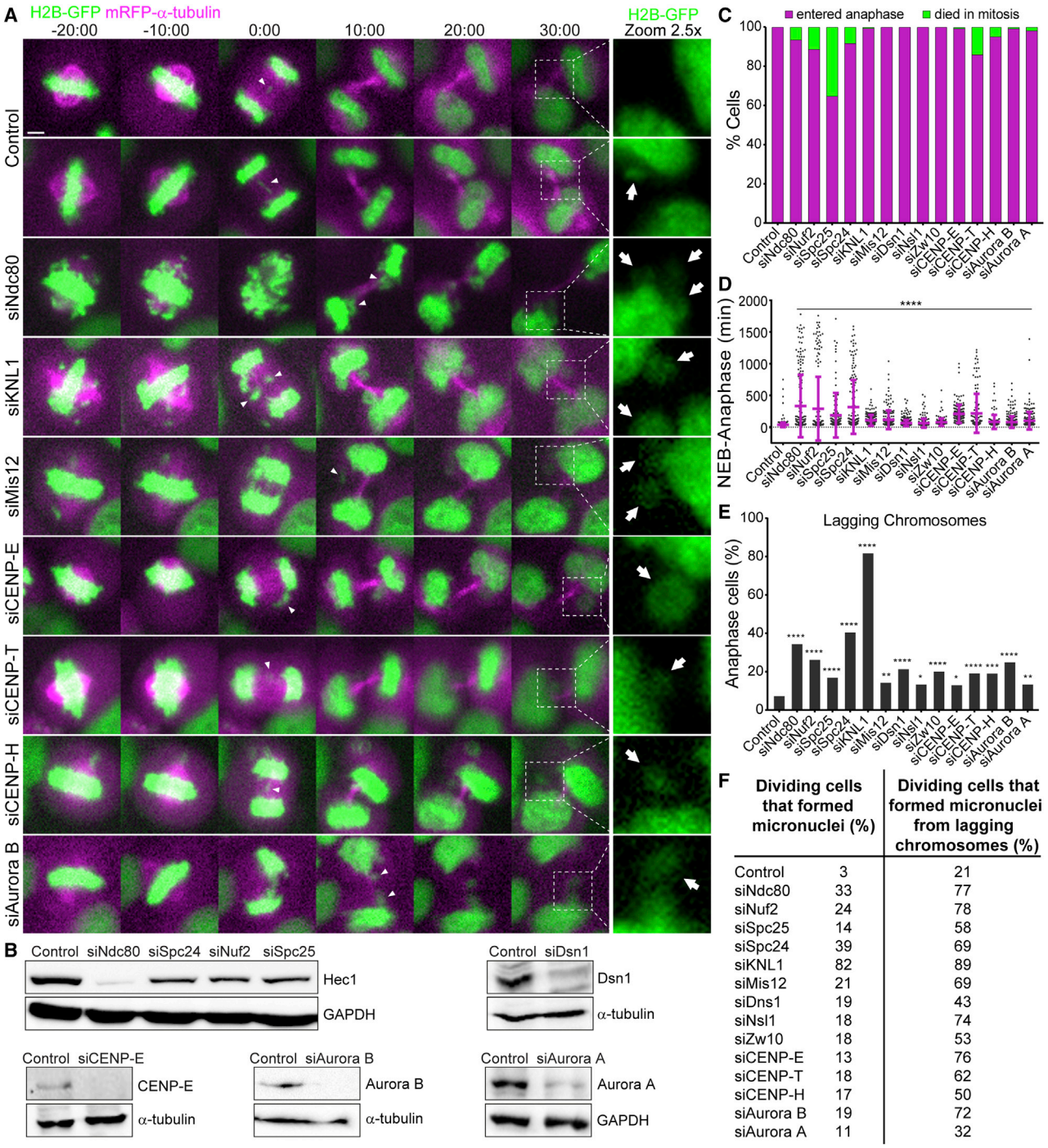

F

	Dividing cells that formed micronuclei (%)	Dividing cells that formed micronuclei from lagging chromosomes (%)
Control	3	21
siNdc80	33	77
siNuf2	24	78
siSpc25	14	58
siSpc24	39	69
siKNL1	82	89
siMis12	21	69
siDns1	19	43
siNsl1	18	74
siZw10	18	53
siCENP-E	13	76
siCENP-T	18	62
siCENP-H	17	50
siAurora B	19	72
siAurora A	11	32

Figure 3. Anaphase error correction and micronuclei prevention requires stable kinetochore-microtubule interactions

(A) HeLa cells stably expressing H2B-GFP and mRFP-α-tubulin treated with scramble small interfering RNA (siRNA) (control) or siNdc80, siKNL1, siMis12, siCENP-E, siCENP-T, siCENP-H, and siAurora B. Time 00:00, anaphase onset. White arrowheads indicate lagging chromosomes and arrows show MN. Scale bar represents 5 μm.

(B) Western blot analysis showing efficient depletion of Ndc80 complex members, Dsn1, CENP-E, Aurora B, and Aurora A after RNAi. GAPDH or α-tubulin were used as loading controls.

(C) Cell fate of mitotic HeLa cells under the specified conditions. Control n = 897, siNdc80 n = 202, siNuf2 n = 204, siSpc25 n = 222, siSpc24 n = 182, siKNL1 n = 194, siMis12 n = 200, siDsn1 n = 459, siNsl1 n = 200, siZw10 n = 187, siCENP-E n = 159, siCENP-T n = 150, siCENP-H n = 125, siAurora B n = 287, and siAurora A n = 229 cells.

(legend continued on next page)

high-throughput screen in live HeLa cells after RNAi-mediated depletion of key KT proteins involved in the formation or regulation of MT attachments, including KMN network components (Cheeseman et al., 2006) and Aurora B (Figures 3A and 3B). Although full depletion of these proteins would be expected to compromise chromosome alignment, segregation, and/or SAC function (Meraldi et al., 2004), we found that the vast majority of cells entered anaphase after a delay and were able to align most chromosomes (Figures 3A, 3C, and 3D), suggesting incomplete depletion. Indeed, western blot analyses using available antibodies against some of the target proteins or complexes confirmed this scenario (Figure 3B). Interestingly, although chromosome alignment and segregation were highly resilient to any experimental condition that partially disrupted KT-MT attachment stability, correction of anaphase lagging chromosomes and their subsequent re-integration into the main nuclei were greatly compromised (Figures 3A, 3E, and 3F). Importantly, the outcome of Aurora B (but not Aurora A) depletion by RNAi was largely indistinguishable from the partial depletion of the KT components tested (Figures 3A, 3E, and 3F), further demonstrating an Aurora-B-specific role in anaphase error correction. Overall, these data suggest that, although centromeric Aurora B promotes MT detachment from KTs under low tension to correct errors in early mitosis (Lampson et al., 2004), midzone-associated Aurora B is required for the local stabilization of KT-MT attachments necessary for efficient mechanical transduction of spindle forces involved in error correction during anaphase.

To directly investigate the impact of a midzone-based Aurora B phosphorylation gradient on KT MT stability, we measured fluorescence dissipation after photoactivation (FDAPA) of GFP-α-tubulin (Girão and Maiato, 2020) in controls and after Mklp2 depletion by RNAi. By fitting the fluorescence decay over time from several cells to a double exponential curve, it is possible to discriminate two spindle MT populations with fast and slow turnover that are thought to correspond to the less stable non-KT MTs and more stable KT MTs, respectively (Bakhoum et al., 2009b; Zhai et al., 1995). Surprisingly, our measurements of FDAPA clearly revealed that both KT and non-KT MTs in control cells still show significant turnover during anaphase, sufficient to renew >50% of KT MTs before the initiation of nuclear envelope reassembly (NER) (Figures 4A–4C), which in U2OS cells takes ~5 min from the onset of anaphase (Figures 5A, 6A, and 6F). Most relevant, we found that Mklp2 depletion caused a slight redistribution in the proportion of KT and non-KT MTs and resulted in a 2-fold reduction on KT MT half-life without significantly affecting non-KT MT half-life relative to controls (Figures 4A–4C).

Lastly, we investigated the molecular mechanism underlying the stabilization of KT-MT attachments by a midzone-based Aurora B phosphorylation gradient. PLK1 is activated at KTs by Aurora-B-mediated phosphorylation at Thr210 (Carmena et al., 2012), and active PLK1 was shown to stabilize KT-MT attachments during early mitosis (Liu et al., 2012). Therefore, we sought to investigate the status of active PLK1 on anaphase lagging chromosomes by using a monoclonal antibody against phosphorylated PLK1 at Thr210 (Tsvetkov and Stern, 2005). We found that, although the overall levels of active PLK1 at anaphase KTs decreased approximately 5-fold relative to prometaphase (our unpublished observations), active PLK1 was specifically enriched at KTs of lagging chromosomes induced by the formation of merotelic attachments after monastrol treatment and washout (Cimini et al., 2003; Thompson and Compton, 2011) in human RPE1 cells (Figures 4D–4F). Taken together, the data from these three distinct, yet complementary, experimental approaches indicate that a midzone-based Aurora B phosphorylation gradient locally stabilizes KT-MT attachments by activating PLK1 at KTs, to promote anaphase error correction and prevent MN formation during human cell division.

A midzone-based Aurora B phosphorylation gradient, rather than microtubule density, spatially controls NER on anaphase lagging chromosomes

We have previously proposed a "chromosome separation checkpoint" in which a constitutive midzone-based Aurora B phosphorylation gradient monitors the extent of chromosome separation during anaphase to spatially control NER (Afonso et al., 2014; Maiato et al., 2015). This model predicts that, in addition to delaying NER during normal chromosome separation in anaphase, a delay of NER on lagging chromosomes would allow anaphase error correction and open a window of opportunity for their subsequent re-integration in the main segregating chromosome mass, where NER is also delayed in the midzone-facing side (Gerlich and Ellenberg, 2003; Lu et al., 2011). To test this prediction, we started by monitoring the Aurora B phosphorylation gradient on chromosomes using a monoclonal antibody against phospho-histone H3 (pH3) on Ser10 in fixed cells, after induction of chromosome segregation errors in RPE1 cells by a 6-h nocodazole treatment and washout (Liu et al., 2018). However, we found that this procedure significantly perturbed the Aurora B phosphorylation gradient in anaphase (Figures S4D–S4F), to an extent equivalent to Mklp2 depletion in human U2OS cells (Figures S4A–S4C). To overcome this limitation, we implemented a high-resolution live-cell microscopy assay to simultaneously image the entire chromosome set labeled either with H2B-mRFP or a Cy3-conjugated Fab fragment against pH3 on Ser10 (Hayashi-Takanaka et al., 2009) and two GFP-tagged non-core NE proteins (Nup153 and LBR) in human U2OS cells, which show an intrinsic high rate of chromosome segregation errors in anaphase. We found that, in striking contrast with controls, the majority of pH3-positive lagging chromosomes and chromosome bridges in Mklp2-depleted cells recruited Nup153 (Figures 5A–5D, 5G, S6A, and S6B; Video S4). Quantitative analyses revealed that,

(D) Quantitative analysis of the time between nuclear envelope breakdown (NEB) and anaphase onset (error bars indicate mean ± SD; analyzed using an unpaired t test).
(E) Frequency of anaphase cells with lagging chromosomes for all conditions (data were pooled from 2 independent experiments, analyzed using the Fisher's exact two-tailed test).
(F) Frequency of dividing cells that form MN (left column) and of dividing cells with lagging chromosomes that form MN (right column).
*$p \leq 0.05$, **$p \leq 0.01$, ***$p \leq 0.001$, and ****$p \leq 0.0001$.

CellPress
OPEN ACCESS

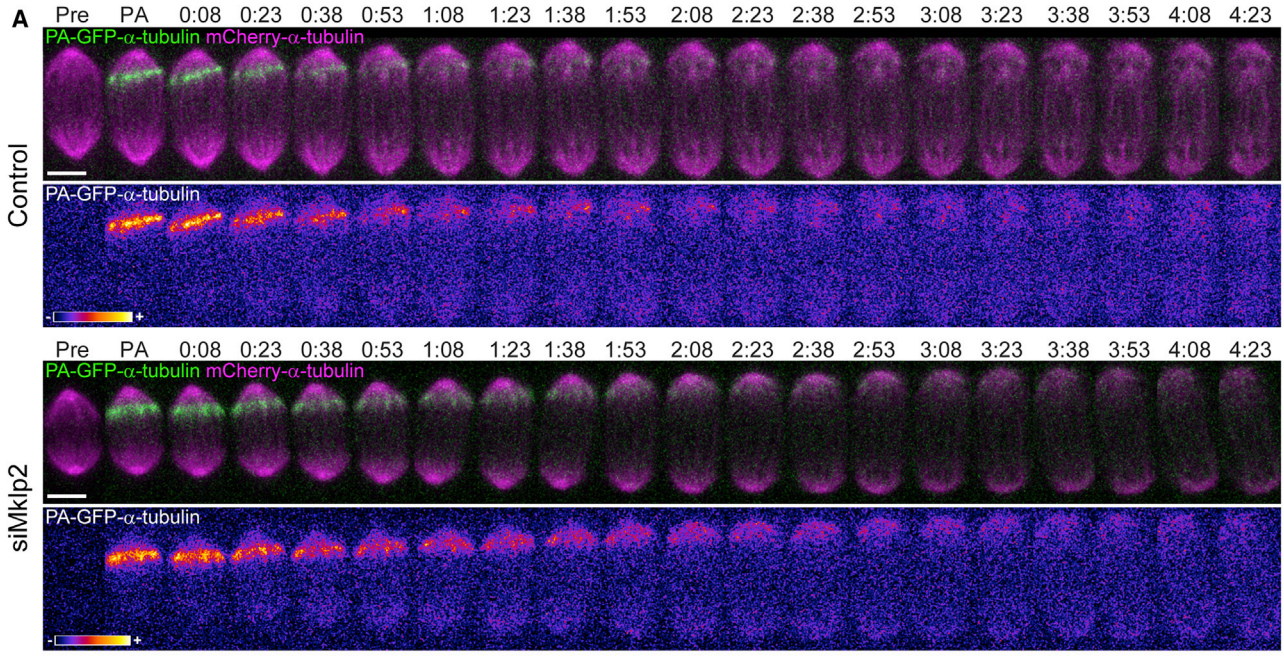

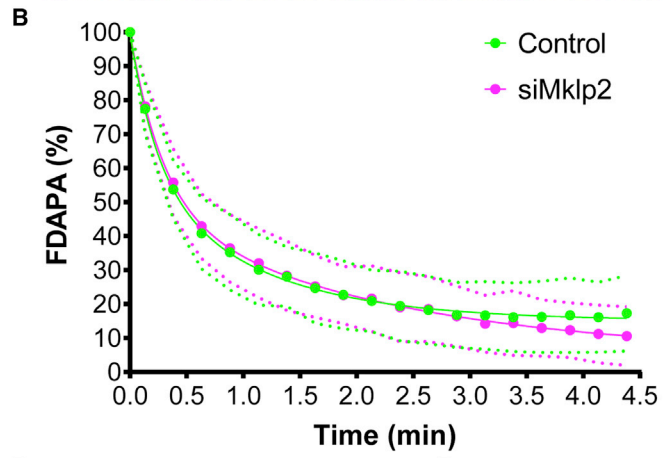

C

	Control	siMklp2	
non-KT MTs (%)	68.1	56.3	(p=0.04)
KT MTs (%)	31.0	43.5	(p=0.029)
non-KT MT half-life (min)	0.27	0.22	(p=0.27)
KT MT half-life (min)	3.97	2.08	(p=0.009)

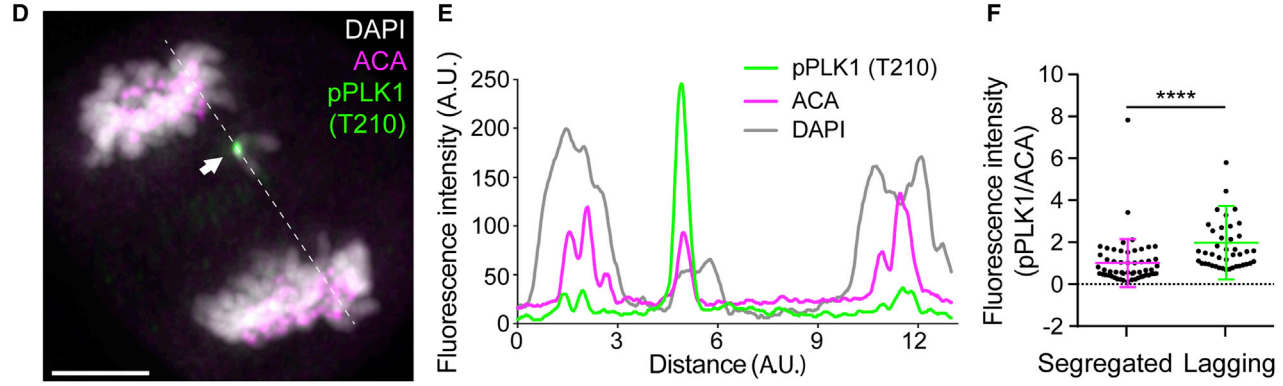

Figure 4. A midzone-based Aurora B phosphorylation gradient stabilizes kinetochore-microtubule attachments during anaphase

(A) Representative examples of control and Mklp2-depleted U2OS cells in anaphase displaying photoactivatable (PA)-GFP-α-tubulin (green) and mCherry-α-tubulin (magenta). PA, frame immediately after photoactivation; pre-PA, frame immediately before photoactivation. PA-GFP-α-tubulin (FIRE LUT) is shown below each cell for better visualization. Scale bar represents 5 μm.

(B) Normalized fluorescence dissipation after photoactivation (FDAPA) curves in control and Mklp2-depleted cells. Whole lines show double exponential curve fittings ($R > 0.99$), and dashed lines show top and bottom SD for each time point.

(legend continued on next page)

as lagging chromosomes in control cells were gradually corrected and moved away from the spindle midzone during anaphase, they began recruiting Nup153 and LBR after a significant delay relative to the main segregating chromosome masses, and this delay was dependent on the establishment of a midzone-based Aurora B phosphorylation gradient (Figures 6A–6E and S7A–S7D; Videos S5 and S6), in line with previous acute Aurora B inhibition experiments in early anaphase (Afonso et al., 2014; Liu et al., 2018). Importantly, we found no discernible delay in the recruitment of core NE components, such as BAF and lamin C, to lagging chromosomes (Figures S7F and S7G), in agreement with previous reports (Liu et al., 2018). Thus, consistent with the transient nature of most anaphase lagging chromosomes, their respective defects in the recruitment of non-core, but not core, NE components are also temporary and may not inevitably result in pathological conditions. Interestingly, Mklp2-depleted cells showed normal Nup153 and LBR recruitment to the main daughter nuclei, despite retaining Aurora B on chromosomes and pH3 for extended periods (Figures 5E, 5F, 6F, and S7E; Videos S5 and S6). This indicates that it is neither the retention of Aurora B on chromosomes nor is pH3 the signal that determines the recruitment of non-core NE proteins, in line with our previous findings in *Drosophila* cells (Afonso et al., 2014). However, a clear correlation between Aurora B activity on lagging chromosomes and Nup153 recruitment was observed in control cells (Figure 5H), and this was dependent on Aurora B localization at the spindle midzone (Figure 5I).

Lastly, to exclude the possible role of MTs in selectively preventing the recruitment of non-core NE components (Liu et al., 2018; Liu and Pellman, 2020), we simultaneously monitored Aurora B activity on chromosomes, Nup153 recruitment, and the distribution of spindle MTs in the same cell over time, with or without Mklp2. We found that Nup153 recruitment to lagging chromosomes after Mklp2 RNAi could not be explained by the disassembly of midzone MTs, as midbodies with high MT density were clearly present and found to co-localize with MN that recruited Nup153 (Figures 7A and 7B; Video S7). Quantitative super-resolution Coherent-Hybrid Stimulated Emission Depletion (CH-STED) analysis in fixed cells (Pereira et al., 2019) confirmed no detectable differences in the density of midzone MT bundles surrounding anaphase lagging chromosomes, with or without Mklp2 (Figures 7C and 7D). We concluded that a midzone-dependent Aurora B phosphorylation gradient, rather than midzone MT density, delays the completion of NER on lagging chromosomes to prevent MN formation in human cells.

DISCUSSION

Mitotic errors are thought to be largely resolved by active correction and surveillance mechanisms that promote proper KT-MT attachments and chromosome bi-orientation prior to anaphase. Importantly, merotelic attachments are still detectable during metaphase (Knowlton et al., 2006), and their correction is promoted by experimentally increasing metaphase duration by 2 h (Cimini et al., 2003), suggesting that few mitotic errors normally escape the surveillance of the SAC that is satisfied within ~20 min upon attachment of the last kinetochore to the spindle (Rieder et al., 1994). The results reported here uncover that this scenario is just the tip of the iceberg, and many more SAC-invisible errors are revealed once the dependence that characterizes all checkpoints is relieved (Hartwell and Weinert, 1989). Indeed, we often found several transient lagging chromosomes in early anaphase in unperturbed cells, with the frequency of anaphase cells with lagging chromosomes, as well as the frequency of lagging chromosomes per cell, rampantly increasing when Aurora B activity or its midzone localization was specifically inhibited after anaphase onset. This increase in lagging chromosomes is unlikely to be due to errors that formed *de novo* after anaphase onset but rather due to compromised error correction during anaphase, unveiling that SAC-invisible errors are more frequent than previously anticipated (see also Sen et al., 2021).

Based on the known roles of Aurora B at centromeres (Cimini et al., 2006; Hauf et al., 2003; Lampson et al., 2004), the proximity to the spindle midzone where Aurora B activity is maximal would be expected to destabilize KT-MT attachments. Although this model might sound appealing, it is difficult to reconcile with the established role of spindle forces in the resolution of merotelic attachments. During this process, KTs first resist spindle forces causing KT deformation and only then merotelic attachments resolve by destabilization of MTs facing the incorrect pole (Cimini et al., 2003, 2004). Here, we show that, in human cells, error correction by spindle forces during anaphase relies on a midzone-based Aurora B phosphorylation gradient that assists kinesin-5-mediated spindle elongation. Moreover, although chromosome alignment and segregation were found to be extremely resilient to partial destabilization of KT-MT attachments, this was detrimental for efficient mechanical transduction of spindle forces required for the correction of anaphase segregation errors and MN prevention. Noteworthy, and in striking contrast to pioneering fluorescence recovery after photobleaching (FRAP) or FDAPA experiments in LLC-PK (pig) and PtK1 (rat kangaroo) cells that showed no or little turnover of KT MTs in anaphase (Gorbsky and Borisy, 1989; Zhai et al., 1995), our direct measurement of KT MT half-life by FDAPA of GFP-α-tubulin revealed that at least 50% of KT MTs are renewed once during the course of anaphase in human cells. Most important, experimental abrogation of the midzone Aurora B phosphorylation gradient caused a 2-fold destabilization of KT MTs and prevented effective anaphase error correction required to

(C) Calculated MT turnover values for control and Mklp2-depleted cells (control n = 28; siMklp2 n = 34; data were pooled from at least 3 independent experiments, analyzed using the Student's t distribution test). p values are indicated between parentheses.
(D) Immunofluorescence analysis of active PLK1 on anaphase lagging chromosomes (white arrow) in RPE1 cells. DAPI (white), anti-centromere antibody (ACA) (magenta), and PLK1 (T210) (green) are indicated. Scale bar represents 5 μm.
(E) Line scan (white dashed line in D) of the cell in (D) quantifying the respective fluorescence intensity (A.U., arbitrary units) of the indicated markers.
(F) Quantification of the fluorescence intensity of pPLK1 (T210) relative to ACAs on segregated versus lagging chromosomes in anaphase (n = 43 lagging and n = 55 segregated chromosomes from 19 cells; data were pooled from at least 3 independent experiments, analyzed using a Mann-Whitney test; error bars indicate mean ± SD; ****$p \leq 0.0001$).

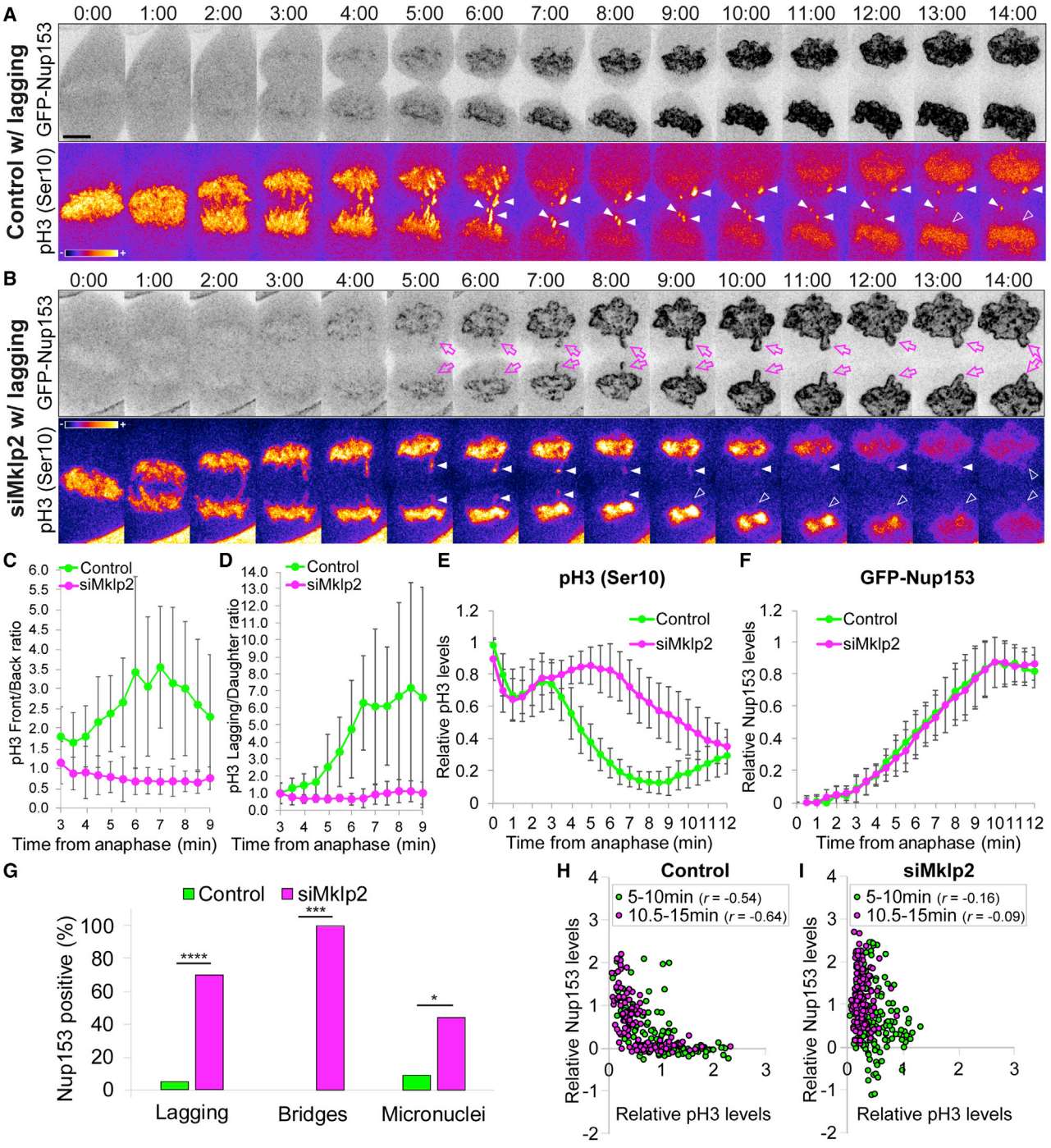

Figure 5. A midzone-based Aurora B phosphorylation gradient spatially regulates the completion of nuclear envelope reassembly on anaphase lagging chromosomes in human cells

(A) Control cell with lagging chromosomes that are negative for Nup153 (inverted, grayscale) and positive for pH3 (FIRE LUT).

(B) Mklp2-depleted cell with lagging chromosomes that are positive for both Nup153 (inverted, grayscale) and pH3 (FIRE LUT). White arrowheads track lagging chromosomes until their eventual re-integration in the main nuclei or form MN. Magenta arrows highlight lagging chromosomes that prematurely accumulate Nup153 in siMklp2-depleted cells. Scale bar represents 5 μm.

(C and D) Quantification of pH3 Ser10 (C) front/back and (D) lagging/daughter ratio on segregating chromosomes during anaphase. Control n = 10; siMklp2 n = 10; error bars represent SD.

(E and F) Quantification of (E) pH3 Ser10 and (F) GFP-Nup153 on daughter chromosomes and nuclei in control and siMklp2-treated cells. Control n = 20; siMklp2 n = 20; error bars represent SD.

(legend continued on next page)

avoid MN. This is consistent with the well-established view that even slight changes in KT MT dynamics may lead to CIN (Bakhoum et al., 2009a, 2009b) and with previous works implicating Aurora B in the stabilization of midzone MTs during anaphase (Ferreira et al., 2013; Nunes Bastos et al., 2013; Uehara et al., 2013). Lastly, we found that active PLK1, which was previously shown to promote the stabilization of KT-MT attachments (Liu et al., 2012), was specifically enriched on anaphase lagging chromosomes. This is in agreement with a role of Aurora B in PLK1 activation at KTs (Carmena et al., 2012) and the decrease in Aurora B activity at KTs as a function of chromosome separation from the spindle midzone (Fuller et al., 2008; Papini et al., 2021). We conclude that anaphase lagging chromosomes actively signal their status to promote error correction and prevent CIN. Taken together, our data support a model in which a midzone-based Aurora B phosphorylation gradient stabilizes KT-MT attachments to promote efficient mechanical transduction of spindle forces involved in the initial step of error correction during anaphase (Figure 7E). This does not exclude that a midzone-based Aurora B phosphorylation gradient regulates additional KT substrates implicated in this or subsequent steps that ultimately lead to the resolution of erroneous KT-MT attachments during anaphase (Papini et al., 2021; Sen et al., 2021).

According to the chromosome separation checkpoint hypothesis (Afonso et al., 2014; Maiato et al., 2015), an anaphase error correction mechanism would not be possible without a coordinated delay in the completion of NER on lagging chromosomes to prevent MN formation. A chromatin-localized Aurora-B-mediated delay in NER has previously been implicated in the prevention of MN formation from late segregating "acentric" chromosomes in *Drosophila* neuroblasts by excluding HP1 from heterochromatin (Warecki and Sullivan, 2018). In this case, late segregating acentric chromosomes remain tethered with the segregated chromosome mass and re-integrate the main nuclei by passing through Aurora-B-dependent channels in the NE (Karg et al., 2015). Here, we show that, in human cells, lagging chromosomes, but not chromosome bridges, are actively corrected by a midzone-dependent Aurora B phosphorylation gradient that locally prevents the completion of NER. Although the local inhibition of NER on both lagging chromosomes and chromosome bridges relies on a midzone phosphorylation gradient, the resolution of bridges might instead rely on Aurora B activity on chromatin, as proposed for tethered acentrics in *Drosophila* neuroblasts (Karg et al., 2015). The specific effect of the midzone Aurora B phosphorylation gradient in the resolution of lagging chromosomes might reflect the nature of the underlying correction mechanism by spindle forces and may be facilitated by localized delays in the completion of NER in the midzone-facing side of the main segregating chromosome mass (Gerlich and Ellenberg, 2003; Lu et al., 2011) to allow re-integration of lagging chromosomes into the main nuclei.

The existence of an active checkpoint-based mechanism that actively monitors chromosome position during anaphase has been recently challenged, and midzone MTs were proposed to act as a passive and selective physical barrier that irreversibly prevents the recruitment of non-core NE components to anaphase lagging chromosomes, independently of Aurora B activity and its midzone localization (Liu et al., 2018). Completion of NER on lagging chromosomes would therefore be strictly dependent on the disassembly of midzone MTs as cells exit mitosis (Liu and Pellman, 2020), with irreversible NE defects on MN emerging as an unsupervised pathological condition that links mitotic errors to chromothripsis. Although the two models are not necessarily mutually exclusive, the interdependence between MTs and Aurora B activity makes it difficult to experimentally separate their respective roles in NE formation. For instance, MT stabilization near chromosomes was shown to depend on Aurora B (Xue et al., 2013) and MTs increase Aurora B kinase activity toward several microtubule-associated substrates *in vitro* (Noujaim et al., 2014). Because Aurora B activity on chromosomes and spindle midzone MTs decreases as a function of chromosome separation during anaphase in live human cells (Fuller et al., 2008; Tan and Kapoor, 2011), it is conceivable that MTs prevent the recruitment of non-core NE proteins to lagging chromosomes by regulating the Aurora-B-dependent phosphorylation of specific substrates on chromatin (e.g., condensin I subunits and/or HP1) or the NE (e.g., lamin B and/or nuclear pore complex proteins; Afonso et al., 2017). Noteworthy, the proposal that midzone MTs, rather than an Aurora B phosphorylation gradient, physically prevent the completion of NER on lagging chromosomes was based on fixed RPE1 cells depleted of Kif4A (a chromokinesin that associates with the spindle midzone in anaphase; Kurasawa et al., 2004), which showed premature accumulation of non-core NE components to lagging chromosomes induced after nocodazole treatment and washout, in striking contrast with Mklp2 depletion (Liu et al., 2018). These findings are at odds with the live-cell data presented here and are difficult to reconcile with the fact that Mklp2 is required for Kif4A accumulation at the spindle midzone (Nunes Bastos et al., 2013; see also Figures S3E–S3G), and Kif4A mediates Aurora B recruitment to this location (Kurasawa et al., 2004). Moreover, our close inspection of spindle midzone MTs in the absence of Mklp2 by super-resolution CH-STED microscopy (Pereira et al., 2019) failed to detect significant differences in MT density in the vicinity of anaphase lagging chromosomes (as well as any significant effect on non-KT MT half-life and spindle elongation capacity, as inferred from spinning disk confocal recordings), in agreement with recent expansion microscopy analysis of human cells depleted of PRC1, which is required for Kif4A recruitment to midzone MTs (Kurasawa et al., 2004; Vukušić et al., 2021). One possibility is that Kif4A spatially controls the completion of NER on lagging chromosomes by

(G) Frequency of mitotic errors that are positive for Nup153 in control and siMklp2-depleted cells (control n = 126 lagging, n = 5 bridges, n = 23 MN; siMklp2 n = 120 lagging, n = 4 bridges, n = 18 MN; data were pooled from at least 3 independent experiments, analyzed using the Fisher's exact two-tailed test; *p $\leq$ 0.05, ***p $\leq$ 0.001, and ****p $\leq$ 0.0001).

(H and I) Correlation between the relative levels of Nup153 and pH3 on lagging chromosomes for (H) control and (I) Mklp2-depleted cells. The calculated Pearson correlation coefficient (*r*) is indicated for each condition and time interval.

See also Figures S4 and S6.

CellPress
OPEN ACCESS

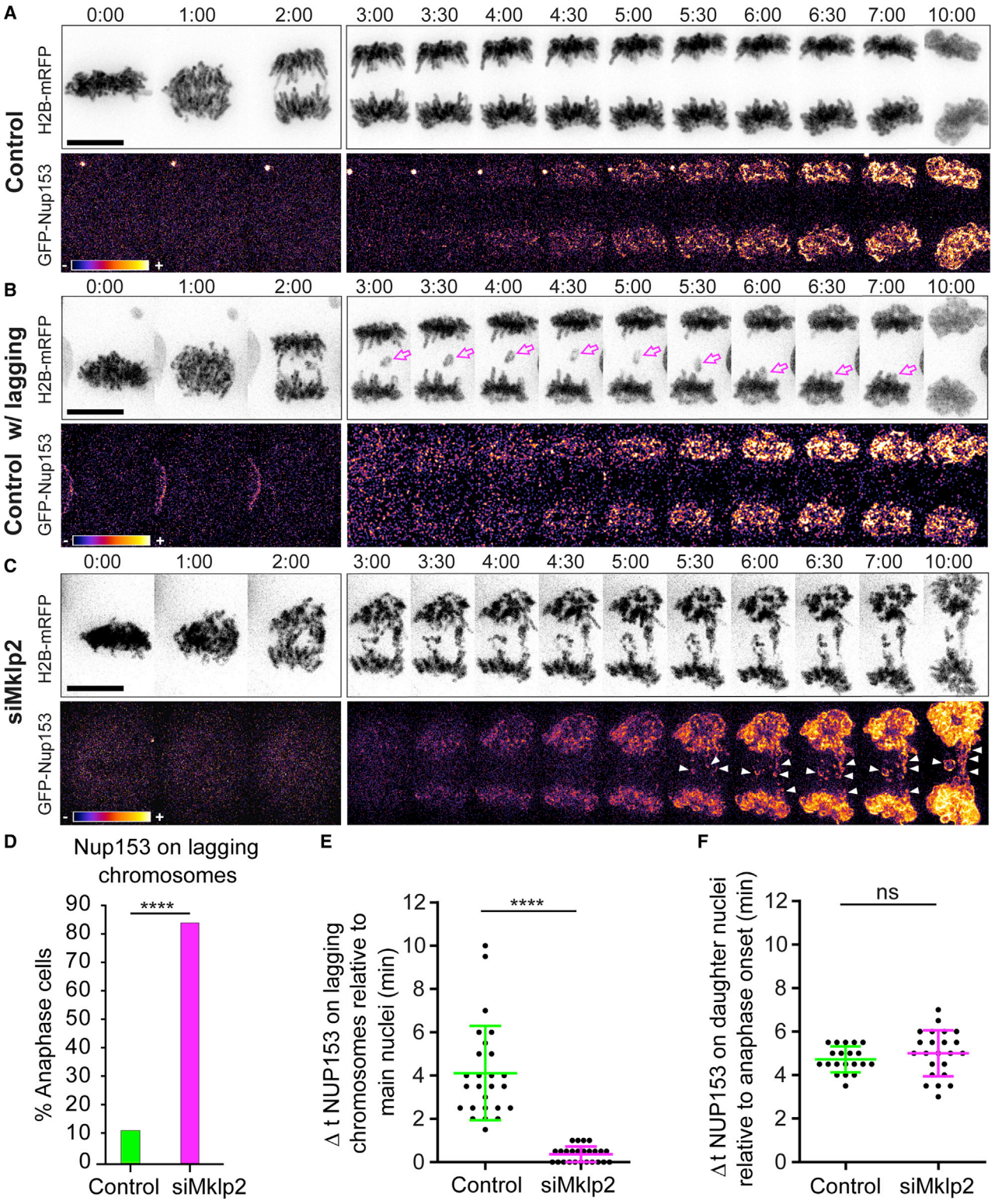

Figure 6. Aurora B midzone localization prevents premature Nup153 accumulation on lagging chromosomes

(A–C) Representative examples of (A) control cell without errors, (B) control cell with a lagging chromosome, and (C) Mklp2-depleted cell with segregation errors. Time is shown in min:s. Cells shown in (A)–(C) are U2OS cells stably expressing mRFP-H2B (inverted; grayscale) and transiently expressing EGFP-Nup153 (FIRE LUT). Scale bar represents 5 μm.

(legend continued on next page)

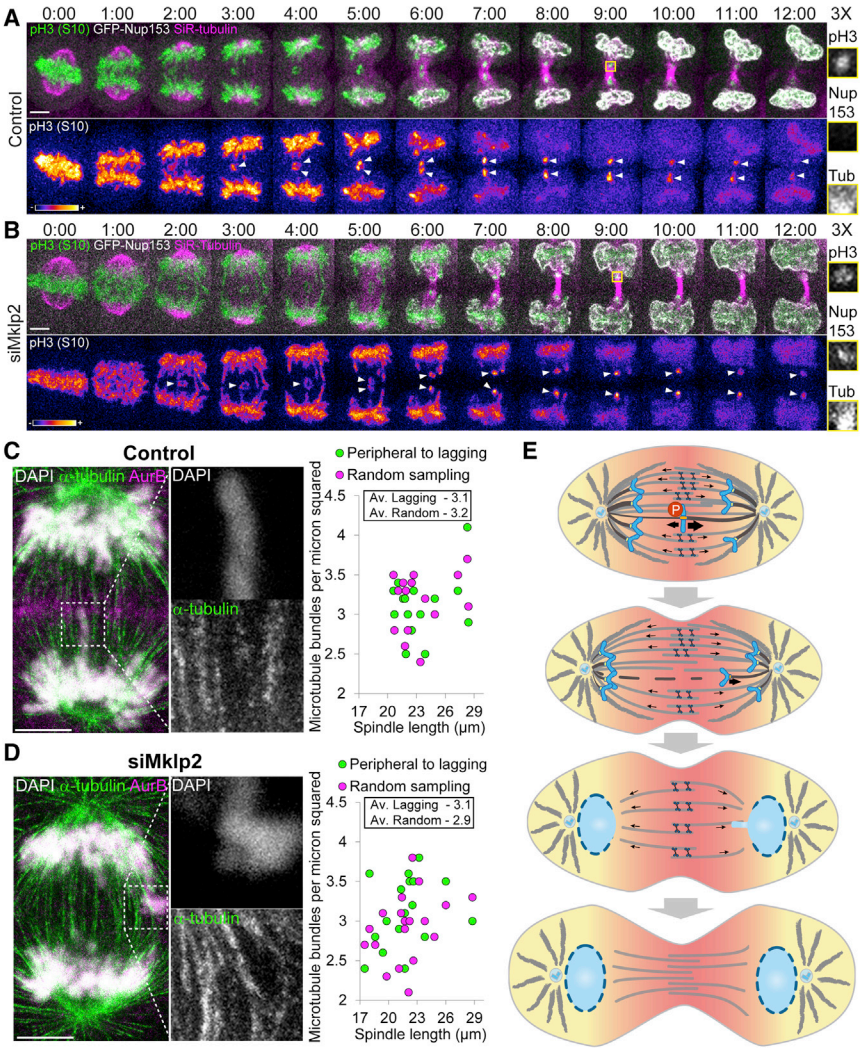

Figure 7. A midzone-based Aurora B phosphorylation gradient prevents premature Nup153 recruitment to lagging chromosomes in the presence of midzone microtubules

(A and B) Representative examples of (A) control and (B) Mklp2-depleted cells displaying pH3 Ser10 (green), GFP-Nup153 (white), and SiR-tubulin (magenta). Scale bars represent 5 μm. pH3 Ser10 alone (FIRE LUT) is shown below each cell for better visualization. White arrowheads track lagging chromosomes until they form MN. Insets show 3× magnification of selected regions with lagging chromosomes (grayscale for single channels of pH3, Nup153, and tubulin).

(C and D) Representative CH-STED images of fixed (C) control and (D) Mklp2-depleted anaphase cells displaying DNA (white), α-tubulin (green), and Aurora B (magenta). Insets show 3× magnification of selected regions with lagging chromosomes (grayscale for single channels of DNA and tubulin). Quantifications on the right show the average number of MT bundles around lagging chromosomes (peripheral to lagging) and at randomly selected regions on the mitotic spindle (random sampling). Each dot represents the average measurement for one cell, and the numbers shown within the black rectangle represent the averages for all cells. Scale bars represent 5 μm.

(E) Proposed model of anaphase error correction and MN prevention by a midzone-based Aurora B phosphorylation gradient (orange and yellow in the cytoplasm). Active PLK1 at KTs is indicated (P). Arrows indicate the direction of spindle forces by kinesin-5 motors crosslinking anti-parallel MTs.

regulating condensin-I-mediated chromosome condensation (Afonso et al., 2014; Mazumdar et al., 2004; Poonperm et al., 2017; Samejima et al., 2012; Takahashi et al., 2016). Furthermore, as we show here, the perturbation of the Aurora B gradient due to unintended effects caused by a prolonged nocodazole treatment and washout cannot be excluded.

Curiously, experiments involving Taxol treatment combined with Aurora B inhibition in late anaphase did favor the idea that midzone MTs, rather than Aurora B activity, prevent the recruitment of non-core NE proteins to chromatin (Liu et al., 2018). However, we show here that Nup153 and LBR recruitment to lagging chromosomes after Mklp2 depletion, as well as Aurora B transport to the spindle midzone in control cells, takes less than 2 min after anaphase onset. Thus, Aurora B inhibition late in anaphase might not be sufficient to revert the phosphorylation gradient that spatially controls NER, which in human cells takes place within 5 min after anaphase onset. Importantly, our high-resolution live-cell assay where Aurora B activity, the recruitment of non-core NE components, and the distribution of mitotic spindle MTs were simultaneously monitored unequivocally demonstrates that a midzone-based Aurora B phosphorylation gradient, rather than midzone MTs per se, delays the completion of NER on lagging chromosomes in human cells.

As in the case of errors that escape the supervision of the SAC, an Aurora-B-dependent chromosome separation checkpoint is not exempt from failure, and a minority of lagging chromosomes

(D) Quantification of the percentage of anaphase cells (control n = 26, siMklp2 n = 25; analyzed using the Fisher's exact two-tailed test) in which Nup153 was detected on lagging chromosomes.

(E) Difference in time (min) between detection of Nup153 on daughter nuclei and lagging chromosomes (control n = 26, siMklp2 n = 25; analyzed using a two-tailed t test; error bars indicate mean ± SD).

(F) Quantification of the time (min) it takes to detect Nup153 on daughter nuclei after anaphase onset (control n = 45, siMklp2 n = 30; analyzed using a two-tailed t test; error bars indicate mean ± SD).

All data were pooled from at least 3 independent experiments. ****$p \leq 0.0001$. See also Figure S7.

might still result in MN. The recent discovery that Aurora-B-mediated phosphorylation of chromatin-associated cGAS prevents its premature activation during mitosis (Li et al., 2021) raises the exciting possibility that an Aurora-B-dependent chromosome separation checkpoint links mechanisms of MN prevention with those involved in the clearance of micronucleated cells to minimize potential detrimental effects. Overall, our findings unveil a layer of protection against genomic instability operating during mitotic exit in human cells, awareness of which will be critical for the rational design of MN-targeting therapies.

STAR★METHODS

Detailed methods are provided in the online version of this paper and include the following:

- KEY RESOURCES TABLE
- RESOURCE AVAILABILITY
  - Lead contact
  - Materials availability
  - Data and code availability
- EXPERIMENTAL MODEL AND SUBJECT DETAILS
  - Cell Culture
- METHOD DETAILS
  - Constructs and Transfections
  - Western Blotting
  - Time-lapse spinning-disk confocal microscopy
  - Immunofluorescence and fixed cell analysis
  - High-content live-cell microscopy screening
  - Stimulated Emission Depletion (STED) microscopy and sample preparation
  - Drug treatments
  - Visualization of histone H3 phosphorylation in living cells
- QUANTIFICATION AND STATISTICAL ANALYSIS
  - Measuring anaphase microtubule turnover by photoactivation
  - Determination of the frequency of lagging chromosomes forming a micronuclei
  - Quantification of mitotic errors
  - Quantification of the Aurora B phosphorylation gradient (Front/Back and Lagging/Daughter ratio)
  - Quantification of spindle elongation, chromosome separation velocity and chromosome separation distance
  - Quantification of pH3 and Nup153 in live cells
  - Statistical Analysis

SUPPLEMENTAL INFORMATION

Supplemental information can be found online at https://doi.org/10.1016/j.celrep.2021.109783.

ACKNOWLEDGMENTS

We thank António Pereira and Ana Almeida for assistance with CH-STED, Ariana Jacome for the generation of lentiviral vectors, Cristina Ferrás and Marco Novais-Cruz for drawing attention to the effects of nocodazole treatment and washout on the Aurora B phosphorylation gradient, current and former lab members for suggestions, and Jonathan Higgins and Andrew McAinsh for discussing results prior to publication. This work was funded by the European Research Council (ERC) consolidator grant CODECHECK, under the European Union's Horizon 2020 research and innovation programme (grant agreement 681443), and Fundação para a Ciência e a Tecnologia of Portugal (PTDC/MED-ONC/3479/2020).

AUTHOR CONTRIBUTIONS

Conceptualization, supervision, project administration, and funding acquisition, H.M.; methodology, B.O., F.D.S., A.M.G., L.T.F., and A.C.F.; investigation, formal analysis, and validation, B.O., F.D.S., A.M.G., and O.A.; visualization, B.O., F.D.S., A.M.G., O.A., and H.M.; writing – original draft, H.M. and B.O.; writing – review and editing, B.O., F.D.S., A.M.G., L.T.F., and H.M.

DECLARATION OF INTERESTS

B.O. declares that he is a consultant specialist at Volastra Therapeutics.

Received: March 1, 2021
Revised: July 15, 2021
Accepted: August 26, 2021
Published: November 9, 2021

REFERENCES

Afonso, O., Matos, I., Pereira, A.J., Aguiar, P., Lampson, M.A., and Maiato, H. (2014). Feedback control of chromosome separation by a midzone Aurora B gradient. Science *345*, 332–336.

Afonso, O., Figueiredo, A.C., and Maiato, H. (2017). Late mitotic functions of Aurora kinases. Chromosoma *126*, 93–103.

Bakhoum, S.F., and Cantley, L.C. (2018). The multifaceted role of chromosomal instability in cancer and its microenvironment. Cell *174*, 1347–1360.

Bakhoum, S.F., Genovese, G., and Compton, D.A. (2009a). Deviant kinetochore microtubule dynamics underlie chromosomal instability. Curr. Biol. *19*, 1937–1942.

Bakhoum, S.F., Thompson, S.L., Manning, A.L., and Compton, D.A. (2009b). Genome stability is ensured by temporal control of kinetochore-microtubule dynamics. Nat. Cell Biol. *11*, 27–35.

Bakhoum, S.F., Silkworth, W.T., Nardi, I.K., Nicholson, J.M., Compton, D.A., and Cimini, D. (2014). The mitotic origin of chromosomal instability. Curr. Biol. *24*, R148–R149.

Bonassi, S., El-Zein, R., Bolognesi, C., and Fenech, M. (2011). Micronuclei frequency in peripheral blood lymphocytes and cancer risk: evidence from human studies. Mutagenesis *26*, 93–100.

Carmena, M., Pinson, X., Platani, M., Salloum, Z., Xu, Z., Clark, A., Macisaac, F., Ogawa, H., Eggert, U., Glover, D.M., et al. (2012). The chromosomal passenger complex activates Polo kinase at centromeres. PLoS Biol. *10*, e1001250.

Cheeseman, I.M., Chappie, J.S., Wilson-Kubalek, E.M., and Desai, A. (2006). The conserved KMN network constitutes the core microtubule-binding site of the kinetochore. Cell *127*, 983–997.

Cimini, D., Howell, B., Maddox, P., Khodjakov, A., Degrassi, F., and Salmon, E.D. (2001). Merotelic kinetochore orientation is a major mechanism of aneuploidy in mitotic mammalian tissue cells. J. Cell Biol. *153*, 517–527.

Cimini, D., Fioravanti, D., Salmon, E.D., and Degrassi, F. (2002). Merotelic kinetochore orientation versus chromosome mono-orientation in the origin of lagging chromosomes in human primary cells. J. Cell Sci. *115*, 507–515.

Cimini, D., Moree, B., Canman, J.C., and Salmon, E.D. (2003). Merotelic kinetochore orientation occurs frequently during early mitosis in mammalian tissue cells and error correction is achieved by two different mechanisms. J. Cell Sci. *116*, 4213–4225.

Cimini, D., Cameron, L.A., and Salmon, E.D. (2004). Anaphase spindle mechanics prevent mis-segregation of merotelically oriented chromosomes. Curr. Biol. *14*, 2149–2155.

Cimini, D., Wan, X., Hirel, C.B., and Salmon, E.D. (2006). Aurora kinase promotes turnover of kinetochore microtubules to reduce chromosome segregation errors. Curr. Biol. *16*, 1711–1718.

Cohen-Sharir, Y., McFarland, J.M., Abdusamad, M., Marquis, C., Bernhard, S.V., Kazachkova, M., Tang, H., Ippolito, M.R., Laue, K., Zerbib, J., et al. (2021). Aneuploidy renders cancer cells vulnerable to mitotic checkpoint inhibition. Nature *590*, 486–491.

Collins, E., Mann, B.J., and Wadsworth, P. (2014). Eg5 restricts anaphase B spindle elongation in mammalian cells. Cytoskeleton (Hoboken) *71*, 136–144.

Courtheoux, T., Gay, G., Gachet, Y., and Tournier, S. (2009). Ase1/Prc1-dependent spindle elongation corrects merotely during anaphase in fission yeast. J. Cell Biol. *187*, 399–412.

Crasta, K., Ganem, N.J., Dagher, R., Lantermann, A.B., Ivanova, E.V., Pan, Y., Nezi, L., Protopopov, A., Chowdhury, D., and Pellman, D. (2012). DNA breaks and chromosome pulverization from errors in mitosis. Nature *482*, 53–58.

Duheron, V., Chatel, G., Sauder, U., Oliveri, V., and Fahrenkrog, B. (2014). Structural characterization of altered nucleoporin Nup153 expression in human cells by thin-section electron microscopy. Nucleus *5*, 601–612.

Fenech, M., Holland, N., Kirsch-Volders, M., Knudsen, L.E., Wagner, K.H., Stopper, H., Knasmueller, S., Bolognesi, C., El-Zein, R., and Bonassi, S. (2020). Micronuclei and disease - report of HUMN project workshop at Rennes 2019 EEMGS conference. Mutat. Res. *850-851*, 503133.

Ferreira, J.G., Pereira, A.J., Akhmanova, A., and Maiato, H. (2013). Aurora B spatially regulates EB3 phosphorylation to coordinate daughter cell adhesion with cytokinesis. J. Cell Biol. *201*, 709–724.

Ferreira, L.T., Figueiredo, A.C., Orr, B., Lopes, D., and Maiato, H. (2018). Dissecting the role of the tubulin code in mitosis. Methods Cell Biol. *144*, 33–74.

Fonseca, C.L., Malaby, H.L.H., Sepaniac, L.A., Martin, W., Byers, C., Czechanski, A., Messinger, D., Tang, M., Ohi, R., Reinholdt, L.G., and Stumpff, J. (2019). Mitotic chromosome alignment ensures mitotic fidelity by promoting interchromosomal compaction during anaphase. J. Cell Biol. *218*, 1148–1163.

Fuller, B.G., Lampson, M.A., Foley, E.A., Rosasco-Nitcher, S., Le, K.V., Tobelmann, P., Brautigan, D.L., Stukenberg, P.T., and Kapoor, T.M. (2008). Midzone activation of aurora B in anaphase produces an intracellular phosphorylation gradient. Nature *453*, 1132–1136.

Gerlich, D., and Ellenberg, J. (2003). 4D imaging to assay complex dynamics in live specimens. Nat. Cell Biol., S14–S19.

Girão, H., and Maiato, H. (2020). Measurement of microtubule half-life and poleward flux in the mitotic spindle by photoactivation of fluorescent tubulin. Methods Mol. Biol. *2101*, 235–246.

Gorbsky, G.J., and Borisy, G.G. (1989). Microtubules of the kinetochore fiber turn over in metaphase but not in anaphase. J. Cell Biol. *109*, 653–662.

Gruneberg, U., Neef, R., Honda, R., Nigg, E.A., and Barr, F.A. (2004). Relocation of Aurora B from centromeres to the central spindle at the metaphase to anaphase transition requires MKlp2. J. Cell Biol. *166*, 167–172.

Guo, X., Ni, J., Liang, Z., Xue, J., Fenech, M.F., and Wang, X. (2019). The molecular origins and pathophysiological consequences of micronuclei: new insights into an age-old problem. Mutat. Res. Rev. Mutat. Res. *779*, 1–35.

Hanahan, D., and Weinberg, R.A. (2000). The hallmarks of cancer. Cell *100*, 57–70.

Haraguchi, T., Kojidani, T., Koujin, T., Shimi, T., Osakada, H., Mori, C., Yamamoto, A., and Hiraoka, Y. (2008). Live cell imaging and electron microscopy reveal dynamic processes of BAF-directed nuclear envelope assembly. J. Cell Sci. *121*, 2540–2554.

Hartwell, L.H., and Weinert, T.A. (1989). Checkpoints: controls that ensure the order of cell cycle events. Science *246*, 629–634.

Hauf, S., Cole, R.W., LaTerra, S., Zimmer, C., Schnapp, G., Walter, R., Heckel, A., van Meel, J., Rieder, C.L., and Peters, J.M. (2003). The small molecule Hesperadin reveals a role for Aurora B in correcting kinetochore-microtubule attachment and in maintaining the spindle assembly checkpoint. J. Cell Biol. *161*, 281–294.

Hayashi-Takanaka, Y., Yamagata, K., Nozaki, N., and Kimura, H. (2009). Visualizing histone modifications in living cells: spatiotemporal dynamics of H3 phosphorylation during interphase. J. Cell Biol. *187*, 781–790.

Hayashi-Takanaka, Y., Yamagata, K., Wakayama, T., Stasevich, T.J., Kainuma, T., Tsurimoto, T., Tachibana, M., Shinkai, Y., Kurumizaka, H., Nozaki, N., and Kimura, H. (2011). Tracking epigenetic histone modifications in single cells using Fab-based live endogenous modification labeling. Nucleic Acids Res. *39*, 6475–6488.

Huang, Y., Jiang, L., Yi, Q., Lv, L., Wang, Z., Zhao, X., Zhong, L., Jiang, H., Rasool, S., Hao, Q., et al. (2012). Lagging chromosomes entrapped in micronuclei are not 'lost' by cells. Cell Res. *22*, 932–935.

Janssen, A., van der Burg, M., Szuhai, K., Kops, G.J., and Medema, R.H. (2011). Chromosome segregation errors as a cause of DNA damage and structural chromosome aberrations. Science *333*, 1895–1898.

Jdey, W., Thierry, S., Popova, T., Stern, M.H., and Dutreix, M. (2017). Micronuclei frequency in tumors is a predictive biomarker for genetic instability and sensitivity to the DNA repair inhibitor AsiDNA. Cancer Res. *77*, 4207–4216.

Karg, T., Warecki, B., and Sullivan, W. (2015). Aurora B-mediated localized delays in nuclear envelope formation facilitate inclusion of late-segregating chromosome fragments. Mol. Biol. Cell *26*, 2227–2241.

Knowlton, A.L., Lan, W., and Stukenberg, P.T. (2006). Aurora B is enriched at merotelic attachment sites, where it regulates MCAK. Curr. Biol. *16*, 1705–1710.

Kurasawa, Y., Earnshaw, W.C., Mochizuki, Y., Dohmae, N., and Todokoro, K. (2004). Essential roles of KIF4 and its binding partner PRC1 in organized central spindle midzone formation. EMBO J. *23*, 3237–3248.

Lampson, M.A., and Grishchuk, E.L. (2017). Mechanisms to avoid and correct erroneous kinetochore-microtubule attachments. Biology (Basel) *6*, E1.

Lampson, M.A., Renduchitala, K., Khodjakov, A., and Kapoor, T.M. (2004). Correcting improper chromosome-spindle attachments during cell division. Nat. Cell Biol. *6*, 232–237.

Li, T., Huang, T., Du, M., Chen, X., Du, F., Ren, J., and Chen, Z.J. (2021). Phosphorylation and chromatin tethering prevent cGAS activation during mitosis. Science *371*, eabc5386.

Liu, S., and Pellman, D. (2020). The coordination of nuclear envelope assembly and chromosome segregation in metazoans. Nucleus *11*, 35–52.

Liu, D., Davydenko, O., and Lampson, M.A. (2012). Polo-like kinase-1 regulates kinetochore-microtubule dynamics and spindle checkpoint silencing. J. Cell Biol. *198*, 491–499.

Liu, S., Kwon, M., Mannino, M., Yang, N., Renda, F., Khodjakov, A., and Pellman, D. (2018). Nuclear envelope assembly defects link mitotic errors to chromothripsis. Nature *561*, 551–555.

Lu, L., Ladinsky, M.S., and Kirchhausen, T. (2011). Formation of the postmitotic nuclear envelope from extended ER cisternae precedes nuclear pore assembly. J. Cell Biol. *194*, 425–440.

Lukinavičius, G., Reymond, L., D'Este, E., Masharina, A., Göttfert, F., Ta, H., Güther, A., Fournier, M., Rizzo, S., Waldmann, H., et al. (2014). Fluorogenic probes for live-cell imaging of the cytoskeleton. Nat. Methods *11*, 731–733.

Ly, P., and Cleveland, D.W. (2017). Rebuilding chromosomes after catastrophe: emerging mechanisms of chromothripsis. Trends Cell Biol. *27*, 917–930.

Mackenzie, K.J., Carroll, P., Martin, C.A., Murina, O., Fluteau, A., Simpson, D.J., Olova, N., Sutcliffe, H., Rainger, J.K., Leitch, A., et al. (2017). cGAS surveillance of micronuclei links genome instability to innate immunity. Nature *548*, 461–465.

Maiato, H., Afonso, O., and Matos, I. (2015). A chromosome separation checkpoint: a midzone Aurora B gradient mediates a chromosome separation checkpoint that regulates the anaphase-telophase transition. BioEssays *37*, 257–266.

Mazumdar, M., Sundareshan, S., and Misteli, T. (2004). Human chromokinesin KIF4A functions in chromosome condensation and segregation. J. Cell Biol. *166*, 613–620.

Meraldi, P., Draviam, V.M., and Sorger, P.K. (2004). Timing and checkpoints in the regulation of mitotic progression. Dev. Cell *7*, 45–60.

Musacchio, A. (2015). The molecular biology of spindle assembly checkpoint signaling dynamics. Curr. Biol. *25*, R1002–R1018.

Norppa, H., and Falck, G.C. (2003). What do human micronuclei contain? Mutagenesis *18*, 221–233.

Noujaim, M., Bechstedt, S., Wieczorek, M., and Brouhard, G.J. (2014). Microtubules accelerate the kinase activity of Aurora-B by a reduction in dimensionality. PLoS ONE *9*, e86786.

Nunes Bastos, R., Gandhi, S.R., Baron, R.D., Gruneberg, U., Nigg, E.A., and Barr, F.A. (2013). Aurora B suppresses microtubule dynamics and limits central spindle size by locally activating KIF4A. J. Cell Biol. *202*, 605–621.

Papini, D., Levasseur, M., and Higgins, J.M.G. (2021). The Aurora B gradient sustains kinetochore stability in anaphase. Cell Rep. *37*. https://doi.org/10.1016/j.celrep.2021.109818.

Pereira, A.J., and Maiato, H. (2010). Improved kymography tools and its applications to mitosis. Methods *51*, 214–219.

Pereira, A., Sousa, M., Almeida, A.C., Ferreira, L.T., Costa, A.R., Novais-Cruz, M., Ferrás, C., Sousa, M.M., Sampaio, P., Belsley, M., and Maiato, H. (2019). Coherent-hybrid STED: high contrast sub-diffraction imaging using a bi-vortex depletion beam. Opt. Express *27*, 8092–8111.

Poonperm, R., Takata, H., Uchiyama, S., and Fukui, K. (2017). Interdependency and phosphorylation of KIF4 and condensin I are essential for organization of chromosome scaffold. PLoS ONE *12*, e0183298.

Rieder, C.L., Schultz, A., Cole, R., and Sluder, G. (1994). Anaphase onset in vertebrate somatic cells is controlled by a checkpoint that monitors sister kinetochore attachment to the spindle. J. Cell Biol. *127*, 1301–1310.

Rozelle, D.K., Hansen, S.D., and Kaplan, K.B. (2011). Chromosome passenger complexes control anaphase duration and spindle elongation via a kinesin-5 brake. J. Cell Biol. *193*, 285–294.

Sablina, A.A., Ilyinskaya, G.V., Rubtsova, S.N., Agapova, L.S., Chumakov, P.M., and Kopnin, B.P. (1998). Activation of p53-mediated cell cycle checkpoint in response to micronuclei formation. J. Cell Sci. *111*, 977–984.

Samejima, K., Samejima, I., Vagnarelli, P., Ogawa, H., Vargiu, G., Kelly, D.A., de Lima Alves, F., Kerr, A., Green, L.C., Hudson, D.F., et al. (2012). Mitotic chromosomes are compacted laterally by KIF4 and condensin and axially by topoisomerase IIα. J. Cell Biol. *199*, 755–770.

Santaguida, S., Richardson, A., Iyer, D.R., M'Saad, O., Zasadil, L., Knouse, K.A., Wong, Y.L., Rhind, N., Desai, A., and Amon, A. (2017). Chromosome mis-segregation generates cell-cycle-arrested cells with complex karyotypes that are eliminated by the immune system. Dev. Cell *41*, 638–651.e5.

Sen, O., Harrison, J.U., Burroughs, N.J., and McAinsh, A.D. (2021). Kinetochore life histories reveal an Aurora-B-dependent error correction mechanism in anaphase. Dev. Cell. https://doi.org/10.1016/j.devcel.2021.10.007.

Shoshani, O., Brunner, S.F., Yaeger, R., Ly, P., Nechemia-Arbely, Y., Kim, D.H., Fang, R., Castillon, G.A., Yu, M., Li, J.S.Z., et al. (2021). Chromothripsis drives the evolution of gene amplification in cancer. Nature *591*, 137–141.

Stephens, P.J., Greenman, C.D., Fu, B., Yang, F., Bignell, G.R., Mudie, L.J., Pleasance, E.D., Lau, K.W., Beare, D., Stebbings, L.A., et al. (2011). Massive genomic rearrangement acquired in a single catastrophic event during cancer development. Cell *144*, 27–40.

Takahashi, M., Wakai, T., and Hirota, T. (2016). Condensin I-mediated mitotic chromosome assembly requires association with chromokinesin KIF4A. Genes Dev. *30*, 1931–1936.

Tan, L., and Kapoor, T.M. (2011). Examining the dynamics of chromosomal passenger complex (CPC)-dependent phosphorylation during cell division. Proc. Natl. Acad. Sci. USA *108*, 16675–16680.

Tcherniuk, S., Skoufias, D.A., Labriere, C., Rath, O., Gueritte, F., Guillou, C., and Kozielski, F. (2010). Relocation of Aurora B and survivin from centromeres to the central spindle impaired by a kinesin-specific MKLP-2 inhibitor. Angew. Chem. Int. Ed. Engl. *49*, 8228–8231.

Thompson, S.L., and Compton, D.A. (2010). Proliferation of aneuploid human cells is limited by a p53-dependent mechanism. J. Cell Biol. *188*, 369–381.

Thompson, S.L., and Compton, D.A. (2011). Chromosome missegregation in human cells arises through specific types of kinetochore-microtubule attachment errors. Proc. Natl. Acad. Sci. USA *108*, 17974–17978.

Tsvetkov, L., and Stern, D.F. (2005). Phosphorylation of Plk1 at S137 and T210 is inhibited in response to DNA damage. Cell Cycle *4*, 166–171.

Uehara, R., Tsukada, Y., Kamasaki, T., Poser, I., Yoda, K., Gerlich, D.W., and Goshima, G. (2013). Aurora B and Kif2A control microtubule length for assembly of a functional central spindle during anaphase. J. Cell Biol. *202*, 623–636.

Vukušić, K., Ponjavić, I., Buđa, R., Risteski, P., and Tolić, I.M. (2021). Microtubule-sliding modules based on kinesins EG5 and PRC1-dependent KIF4A drive human spindle elongation. Dev. Cell *56*, 1253–1267.e10.

Warecki, B., and Sullivan, W. (2018). Micronuclei formation is prevented by Aurora B-mediated exclusion of HP1a from late-segregating chromatin in *Drosophila*. Genetics *210*, 171–187.

Worrall, J.T., Tamura, N., Mazzagatti, A., Shaikh, N., van Lingen, T., Bakker, B., Spierings, D.C.J., Vladimirou, E., Foijer, F., and McClelland, S.E. (2018). Non-random mis-segregation of human chromosomes. Cell Rep. *23*, 3366–3380.

Xue, J.Z., Woo, E.M., Postow, L., Chait, B.T., and Funabiki, H. (2013). Chromatin-bound Xenopus Dppa2 shapes the nucleus by locally inhibiting microtubule assembly. Dev. Cell *27*, 47–59.

Zhai, Y., Kronebusch, P.J., and Borisy, G.G. (1995). Kinetochore microtubule dynamics and the metaphase-anaphase transition. J. Cell Biol. *131*, 721–734.

Zhang, C.Z., Spektor, A., Cornils, H., Francis, J.M., Jackson, E.K., Liu, S., Meyerson, M., and Pellman, D. (2015). Chromothripsis from DNA damage in micronuclei. Nature *522*, 179–184.

STAR★METHODS

KEY RESOURCES TABLE

REAGENT or RESOURCE	SOURCE	IDENTIFIER
Antibodies		
rabbit anti-Mklp2/Kif20A	Bethyl Laboratories	Cat#A300-879A; RRID:AB_2131560
rabbit anti-phospho Aurora A/B/C (T288/232/398)	Cell Signaling Technology	Cat#2914; RRID:AB_2061631
rabbit anti-Phospho-Histone H3 Ser10 (Monoclonal; D2C8)	Cell Signaling Technology	Cat#3377; RRID:AB_1549592
mouse anti-pPLK1 T210 (Monoclonal)	ABCAM	Cat# ab39068; RRID:AB_10861033
mouse anti-GAPDH (Monoclonal)	Proteintech	Cat#10494-1-AP; RRID:AB_2263076
Human anti-centromere antibodies	Fitzgerald	Cat#90C-CS1058; RRID:AB_1282595
rabbit anti-HRP	Jackson ImmunoResearch	Cat#111-035-003; RRID:AB_2313567
mouse anti-HRP	Jackson ImmunoResearch	Cat#115-035-003; RRID:AB_10015289
mouse anti-Aurora B (Monoclonal AIM-1)	BD Biosciences	Cat#611082; RRID:AB_2227708
mouse anti-INCENP (Monoclonal)	Santa Cruz Biotechnology	Cat#sc-376514; RRID:AB_11149761
rabbit anti-Kif4a	Thermofisher	Cat#PA5-30492; RRID:AB_2547966
anti-rabbit Alexa Fluor 488	Thermofisher	Cat#A27034; RRID:AB_2536097
anti-mouse Alexa Fluor 568	Thermofisher	Cat#A-11004; RRID:AB_2534072
rat monoclonal anti-tyrosinated α-tubulin clone YL1/2	Bio-Rad	Cat#MCA77G; RRID:AB_325003
anti-mouse STAR-580	Abberior	Cat#2-0002-005-1; RRID:AB_2620153
anti-rat STAR-RED	Abberior	Cat#2-0132-011-2; RRID: AB_2810982
Fab311-Cy3 (Fab antibody fragment that recognizes phosphorylation of Serine 10 on Histone H3)	Hayashi-Takanaka et al., 2011	N/A
Chemicals, peptides, and recombinant proteins		
ZM447439 (Aurora kinase inhibitor)	Selleckchem	Cat#S1103
		CAS: 331771-20-1
Paprotrain	Tocris Bioscience	CAS: 57046-73-8
SiR-Tubulin	Spirochrome	Cat#251SC002
FCPT (Eg5 inhibitor)	Tim Mitchison (MA, USA)	N/A
Nocodazole	Sigma-Aldrich	Cat#M1404
Monastrol	Tocris Bioscience	CAS: 254753-54-3
Experimental models: cell lines		
Human: U2OS	Stephen Geley (Innsbruck, Austria)	N/A
Human: U2OS H2B-eGFP/mCherry-α-tubulin	Stephen Geley (Innsbruck, Austria)	N/A
Human: hTERT-RPE1 (RPE1) parental	ATCC	ATCC® CRL-4000
Human: HeLa LAP-Aurora B	Ben Black (U. Pennsylvania, PA, USA)	N/A
Human: U2OS mRFP-H2B	This paper	N/A
Human: hTERT-RPE1 H2B-eGFP/mCherry-α-tubulin	This paper	N/A
Human: U2OS eGFP-Nup153	This paper	N/A
Human: U2OS mRFP-H2B/eGFP-Lamin C	This paper	N/A
Human: U2OS mRFP-H2B/eGFP-BAF	This paper	N/A
Oligonucleotides		
siRNA targeting sequence for Mklp2: AA CGAACUGCUUUAUGACCUA	Sigma Aldrich	N/A

(*Continued on next page*)

Continued

REAGENT or RESOURCE	SOURCE	IDENTIFIER
siRNA targeting sequence for Control (scramble): UGGUUUACAUGUCGACUAA	Sigma Aldrich	N/A
siRNA targeting sequence for Nuf2: AAGCAUGCCGUGAAACGUAUA[dT][dT]	Sigma Aldrich	N/A
siRNA targeting sequence for Ndc80: GAAUUGCAGCAGACUAUUA[dT][dT]	Sigma Aldrich	N/A
siRNA targeting sequence for Spc24: CUCAACUUUACCACCAAGUUA[dT][dT],	Sigma Aldrich	N/A
siRNA targeting sequence for Spc25: CUGCAAAUAUCCAGGAUCU[dT][dT],	Sigma Aldrich	N/A
siRNA targeting sequence for KNL1: GCAUGUAUCUCUUAAGGAA[dT][dT],	Sigma Aldrich	N/A
siRNA targeting sequence for Mis12: GAAUCAUAAGGACUGUUCA[dT][dT],	Sigma Aldrich	N/A
siRNA targeting sequence for Dsn1: GUCUAUCAGUGUCGAUUUA[dT][dT],	Sigma Aldrich	N/A
siRNA targeting sequence for Nsl1: CAUGAGCUCUUUCUGUUUA[dT][dT],	Sigma Aldrich	N/A
siRNA targeting sequence for Zw10: UGAUCAAUGUGCUGUUCAA[dT][dT],	Sigma Aldrich	N/A
siRNA targeting sequence for CENP-E: GAACUAAGAAGAAGCGUAU[dT][dT],	Sigma Aldrich	N/A
siRNA targeting sequence for CENP-T: CAGUAGUGGCCAGGCUUCA[dT][dT],	Sigma Aldrich	N/A
siRNA targeting sequence for CENP-H: UGGUUGAUGCAAGUGAAGA[dT][dT],	Sigma Aldrich	N/A
siRNA targeting sequence for Aurora A: AUGCCCUGUCUUACUGUCA[dT][dT],	Sigma Aldrich	N/A
siRNA targeting sequence for Aurora B: AACGCGGCACUUCACAAUUGA[dT][dT	Sigma Aldrich	N/A
Recombinant DNA		
eGFP-LBR	Tokuko Haraguchi (Kobe, Japan)	N/A
eGFP-BAF	Tokuko Haraguchi (Kobe, Japan)	N/A
pEGFP(C3)-Nup153	Duheron et al., 2014	Addgene #64268
Software and algorithms		
ImageJ	N/A	https://imagej.nih.gov/ij/
Nikon Elements	Nikon Instruments Inc.	https://www.microscope.healthcare.nikon.com/products/software/nis-elements

RESOURCE AVAILABILITY

Lead contact

Further information and requests for resources and reagents should be directed to and will be fulfilled by the Lead Contact, Helder Maiato (maiato@i3s.up.pt).

Materials availability

All unique reagents generated in this study are available from the Lead Contact without restriction.

Data and code availability

- All data reported in this paper will be shared by the lead contact upon request.
- This paper does not report original code.
- Any additional information required to reanalyze the data reported in this paper is available from the lead contact upon request.

EXPERIMENTAL MODEL AND SUBJECT DETAILS

Cell Culture

All cell lines were cultured at 37°C in 5% CO_2 atmosphere in Dulbecco's modified medium (DMEM; GIBCO, Thermofisher) containing 10% fetal bovine serum (FBS; GIBCO, Thermofisher). U2OS parental, H2B-eGFP/mCherry-α-tubulin and photoactivatable(PA)-GFP-α-tubulin/mCherry-α-tubulin U2OS cells were kindly provided by S. Geley (Innsbruck Medical University, Innsbruck, Austria) and R. Medema (NKI, Amsterdam, the Netherlands). hTERT-RPE1 (RPE1) parental (ATCC® CRL-4000) and HeLa LAP-Aurora B cells kindly provided by Ben Black (U. Pennsylvania, PA, USA). Stable mRFP-H2B U2OS, mRFP-H2B/eGFP-Lamin C U2OS and H2B-eGFP/mCherry-α-tubulin RPE1 cells were generated by lentiviral transduction as previously described (Ferreira et al., 2018). Stable eGFP-Nup153 U2OS cells were generated through transfection of an eGFP-Nup153 plasmid using Lipofectamine 2000 according to the manufacturer instructions. Single cell clones were expanded and assayed for correct localization and moderate expression levels. One clone was processed using Fluorescence Activated Cell Sorting (FACS; FACS Aria II) and selected for use as a stable cell line throughout this study.

METHOD DETAILS

Constructs and Transfections

To express fluorescently-tagged proteins, cells were transfected using Lipofectamine 2000 (Thermofisher) with 1 μg of each construct. Plasmids used were: pEGFP(C3)-Nup153 was a gift from Birthe Fahrenkrog (Addgene plasmid # 64268; http://addgene.org/64268; RRID:Addgene_64268) (Duheron et al., 2014); eGFP-LBR and eGFP-BAF, kindly provided by Tokuko Haraguchi (Advanced ICT Research Institute Kobe, NICT, Kobe, Japan) (Haraguchi et al., 2008); Lentiviral eGFP-Lamin C construct was generated by PCR amplification of eGFP-Lamin C, with introduction of KpnI and XbaI restriction sites, and used subsequently for cloning into a third generation PRRL-CMV expression plasmid. To deplete Mklp2 by RNA interference (RNAi), cells were plated at 40%–50% confluence onto 22 × 22 mm No. 1.5 glass coverslips and cultured for 12 h in DMEM supplemented with 10% of FBS before transfection. Cells were starved in serum-free media (Opti-MEM, Thermofisher) by incubating 1 h before RNAi transfection. RNAi transfection was performed using Lipofectamine RNAiMAX reagent (Thermofisher) with 25 nM of validated siRNA oligonucleotides against human Mklp2: 5′-AACGAACUGCUUUAUGACCUA-3′ (Sigma Aldrich) and control (scramble) siRNA 5′-UGGUUUACAUGUCGAC UAA-3′ (Sigma Aldrich), diluted in serum-free media (Opti-MEM, Thermofisher). Untreated, mock transfected or scramble siRNA results were indistinguishable and were therefore referred to as Control. Depletion of Mklp2 was maximal at 72h after siRNA transfection and all of the analysis was performed at 72h.

Western Blotting

Cell extracts were collected after trypsinization and centrifuged at 1200 rpm for 5 min, washed and re-suspended in Lysis Buffer (NP-40, 20 nM HEPES/KOH pH 7.9 ; 1 mM EDTA pH 8; 1 mM EGTA; 150 mM NaCl; 0.5% NP40; 10% glycerol, 1:50 protease inhibitor; 1:100 Phenylmethylsulfonyl fluoride). The samples were then flash frozen in liquid nitrogen and kept on ice for 30 min. After centrifugation at 14000 rpm for 10 min at 4°C the supernatant was collected and protein concentration determined by the Bradford protein assay (Bio-Rad). The proteins were run on SDS-PAGE gels (50 μg per lane) and transferred at constant amperage for 10 min using the iBlot Gel Transfer Device (Thermo Scientific), to a nitrocellulose Hybond-C membrane. Membranes were then blocked with 5% Milk in TBS with 0.1% Tween-20 (TBS-T) for 1 h at room temperature. The primary antibodies used were: anti-rabbit Mklp2/Kif20A (Bethyl Laboratories; 1:5000); anti-rabbit phospho Aurora A/B/C (T288/232/398; Cell Signaling; 1:2000); anti-rabbit Phospho-Histone H3 Ser10 (Monoclonal; D2C8; Cell Signaling Technology; 1:5000); anti-mouse Hec1 (9GA) (Monoclonal; Abcam; 1:1000), anti-mouse Dsn1 (a gift from A. Musacchio, 1:500), anti-mouse CENP-E (Monoclonal; Santa Cruz Biotechnology; 1:500), anti-mouse Aurora B (Monoclonal, BD Bioscience, 1:1000), anti-mouse GAPDH (Monoclonal; Proteintech; 1:40000), anti-mouse α-tubulin (Monoclonal; Sigma, 1:5000). All primary antibodies were incubated overnight at 4°C with shaking. After three washes in TBS-T the membranes were incubated with the secondary antibody for 1-3 h at room temperature. The secondary antibodies used were anti-mouse-HRP (Jackson ImmunoResearch) and anti-rabbit-HRP (Jackson ImmunoResearch) at 1:5000. After several washes with TBS-T, the detection was performed with Clarity Western ECL Substrate (Bio-Rad).

Time-lapse spinning-disk confocal microscopy

For time-lapse microscopy, cells were plated onto 22 × 22 mm (No. 1.5) glass coverslips (Corning) and cell culture medium was changed to DMEM with 10% FBS (without phenol red and supplemented with HEPES buffer) 6-12 h before mounting. Coverslips were mounted onto 1-well Chamlide CMS imaging chambers (Microsystem AB; Sweden) immediately before imaging. All live-cell imaging experiments were performed at 37°C using temperature-controlled Nikon TE2000 microscopes equipped with a modified Yokogawa CSU-X1 spinning-disc head (Yokogawa Electric), an electron multiplying iXon+ DU-897 EM-CCD camera (Andor) and a filter-wheel. Three laser lines were used for excitation at 488, 561 and 647nm. All live cell imaging experiments were performed using an oil-immersion 100x 1.4 NA Plan-Apo DIC (Nikon), with the exception of the experiments conducted with co-expression of Fab311-Cy3 and eGFP-Nup153, that were performed using an oil-immersion 60x 1.4 NA Plan-Apo DIC (Nikon). All image acquisition was controlled by NIS Elements AR software. Images were collected every 30 s: 9 × 2 μm z stacks spanning a total volume of 16 μm.

Immunofluorescence and fixed cell analysis

For immunofluorescence processing, cells were fixed with 4% Paraformaldehyde (Electron Microscopy Sciences) for 10 min followed by extraction with 2 × 5 min washes using 0.5% Triton X-100 (Sigma-Aldrich). Primary antibodies used were: anti-mouse Aurora B (Monoclonal AIM-1; BD Biosciences; 1:250); anti-mouse INCENP (Monoclonal; Santa Cruz Biotechnology; 1:50); anti-rabbit Mklp2/Kif20A (Bethyl Laboratories; 1:2000); anti-rabbit Phospho-Histone H3 Ser10 (Monoclonal; D2C8; Cell Signaling Technology; 1:5000), anti-rabbit Kif4a (Thermofisher; 1:1000); human anti-centromere antibodies (1:2000; Fitzgerald); mouse anti-pT210 PLK1 (1:1000; Abcam). Secondary antibodies used were Alexa Fluor 488 (Themofisher; 1:2000) and Alexa Fluor 568 (Themofisher; 1:2000). DNA was counterstained with 1 μg/mL DAPI (4',6'-diamino-2-fenil-indol; Sigma-Aldrich) and mounted onto glass slides with 20 mM Tris pH8, 0.5 N-propyl gallate and 90% glycerol. 3D wide-field images were acquired using an AxioImager Z1 (100x Plan-Apochromatic oil differential interference contrast objective lens, 1.46 NA, ZEISS) equipped with a CCD camera (ORCA-R2, Hamamatsu) operated by Zen software (ZEISS). Blind deconvolution of 3D image datasets was performed using Autoquant X software (Media Cybernetics).

High-content live-cell microscopy screening

HeLa cells stably expressing GFP-H2B/mRFP-α-tubulin were plated onto 96-well plate in DMEM supplemented with 5% FBS and after 1 h transfected with siRNA oligonucleotides against human Nuf2:AAGCAUGCCGUGAAACGUAUA[dT][dT], Ndc80:GAAUUGCAGCAGACUAUUA[dT][dT], Spc24:CUCAACUUUACCACCAAGUUA[dT][dT], Spc25:CUGCAAAUAUCCAGGAUCU[dT][dT], KNL1:GCAUGUAUCUCUUAAGGAA[dT][dT], Mis12:GAAUCAUAAGGACUGUUCA[dT][dT], Dsn1:GUCUAUCAGUGUCGAUUUA[dT][dT], Nsl1:CAUGAGCUCUUUCUGUUUA[dT][dT],

Zw10:UGAUCAAUGUGCUGUUCAA[dT][dT],
CENP-E: GAACUAAGAAGAAGCGUAU[dT][dT],
CENP-T: CAGUAGUGGCCAGGCUUCA[dT][dT],
CENP-H: UGGUUGAUGCAAGUGAAGA[dT][dT]
Aurora B: AACGCGGCACUUCACAAUUGA[dT][dT],

Aurora A: AUGCCCUGUCUUACUGUCA[dT][dT] at a final concentration of 50 nM. Transfections were performed using Lipofectamine RNAiMAX in Opti-MEM medium (both from Thermo Fisher Scientific) according to the manufacturer's instructions. Transfection medium was replaced with complete medium after 6 h. Phenotypes were analyzed and quantified between 24 to 72 h later depending on RNAi depletion efficiency as monitored by the percentage of mitotic cells and by western botting (data not shown). For time-lapse microscopy acquisition, cell culture medium was changed to DMEM with 10% FBS without phenol red and supplemented with HEPES buffer) 6-12 h before acquisition. The image acquisition was performed in an INCell Analyzer 2000 (GE Healthcare, Chicago, IL, USA) with a Nikon 20x/0.45 NA Plan Fluor objective according to manufacturer instructions. Images were collected every 10 min for 72 h.

Stimulated Emission Depletion (STED) microscopy and sample preparation

For the best visualization of microtubules, cells were fixed with a solution of 4% Paraformaldehyde (Electron Microscopy Sciences) with 0.25% Glutaraldehyde (Electron Microscopy Sciences) for 10 min, followed by quenching of autofluorescence using 0.1% Sodium Borohydride (Sigma-Aldrich) for 10 min. Cells were then permeabilized by washing 2 × 5 min with PBS 0.5% Triton X-100 (Sigma-Aldrich). Primary antibodies used were: mouse anti-Aurora B (Monoclonal AIM-1; BD Biosciences; 1:250); rat monoclonal anti-tyrosinated α-tubulin clone YL1/2 (Bio-Rad, 1:100). STAR-580 (1:100, Abberior), and STAR-RED (1:100, Abberior) were used as secondary antibodies, and DNA was counterstained with 1 μg/ml DAPI (Sigma-Aldrich). For Coherent-Hybrid STED (CH-STED) imaging (Pereira et al., 2019), an Abberior 'Expert Line' gated-STED microscope was used, equipped with a Nikon Lambda Plan-Apo 1.4 NA 60x objective lens. The depletion beam was generated by a bivortex phase mask (radii ratio = 0.88) to improve suppression of background fluorescence in comparison to conventional 2D-STED. This performance stems from the capacity of a bivortex to generate a depletion dip in 3D that, unlike z-STED or 2D+z-STED combinations, preserves resilience to spherical aberration. All acquisition channels (confocal and STED) were performed using a 0.8 Airy unit pinhole. A time-gate threshold of 500 ps was applied to the STED channel.

Drug treatments

For live visualization of the mitotic spindle in eGFP-Nup153 U2OS cells, SiR-Tubulin (50 nM; Spirochrome) (Lukinavičius et al., 2014) was added to the culture medium 30 min-1 h before acquisition. For acute inhibition of Aurora B activity, ZM447439 (Sigma-Aldrich) was used at 1 μM for U2OS and 2 μM for RPE1 cells. For acute inhibition of Aurora B midzone relocalization, Paprotrain (Tocris Bioscience) was used at 10 μM. For inhibition of spindle elongation, FCPT (kind gift from Tim Mitchison, Harvard University, MA, USA) was used at 100 μM. For all live cell experiments, ZM447439, Paprotrain and FCPT were added within the first min after anaphase onset and DMSO was used as a control. For nocodazole washout experiments to induce lagging chromosomes RPE1 cells were treated with 100 ng/mL Nocodazole (Sigma-Aldrich) for 6 h as previously described (Liu et al., 2018). Nocodazole was washed out by rinsing twice with PBS followed by incubation in fresh DMEM with 10% FBS. Cells were fixed and processed for immunofluorescence 40 min

after the Nocodazole was washed out. For induction of lagging chromosomes with merotelic attachments in RPE1 cells, a monastrol washout assay was performed according to previous reports (Thompson and Compton, 2011). Briefly, cells were incubated during 8-10 h with 100 μM monastrol. After this period, monastrol was washed twice with warm PBS followed by washing with warm fresh medium. Entry in anaphase was monitored under the microscope and cells were processed for fixation after the wave of anaphase figures was observed, typically around 50-60 min after washout.

Visualization of histone H3 phosphorylation in living cells

For visualization of phosphorylation of histone H3 on Serine 10 in living cells, U2OS cells were loaded with a fluorescently labeled specific Fab antibody fragment that recognizes phosphorylation of Serine 10 on Histone H3 (Fab311-Cy3). U2OS cells were at 80%–100% confluence at the time of delivery. For each 22 × 22 mm coverslip, 2 μL of 0.5 mg/ml Fab311-Cy3 were loaded using glass beads (Hayashi-Takanaka et al., 2011) and re-grown in DMEM supplemented with 10% FBS (without phenol red and supplemented with HEPES buffer) for 6-8 h prior to imaging.

QUANTIFICATION AND STATISTICAL ANALYSIS

Measuring anaphase microtubule turnover by photoactivation

Microtubule turnover was measured in U2OS cells stably expressing PA-GFP-α-tubulin /mCherry-α-tubulin seeded on glass coverslips. Cells were followed through mitosis by tracking the mitotic spindle (mCherry- α-tubulin) and were photoactivated within 1min of anaphase onset. Microtubules were locally activated in a thin stripe of ~1 μm width spanning one half-spindle in an area mid-way between the spindle pole and the chromosomes. The 405 nm mosaic laser was used at 75% power and cells were pulsed once (500 ms exposure). Seven 1-μm fluorescence image stacks were captured with a 100X oil-immersion 1.4 numerical aperture objective every 15 s for 4:30 min. To quantify fluorescence dissipation after photoactivation (FDAPA), whole-spindle sum-projected kymographs (sum projections generated using ImageJ and kymographs generated as previously described in Pereira and Maiato (2010) were quantified using a using a custom-written routine in MATLAB and intensities were normalized to the first time-point after photoactivation (following background subtraction from the respective non-activated half-spindle). Photobleaching correction was performed by normalizing to the fluorescence loss of whole-cell (including cytoplasm), sum projected images (i.e., a bleaching constant was calculated for each cell). To calculate MT turnover, the normalized intensity values at each time point (corrected for photobleaching) were fitted to a double exponential curve A1*exp(-k1*t) + A2*exp(-k2*t) using MATLAB (Mathworks), in which t is time, A1 represents the less stable (non-KT MTs) population and A2 the more stable (KT-MTs) population with decay rates of k1 and k2, respectively (R squared value > 0.99). From these curves, the rate constants and the percentage of MTs for the fast (typically interpreted as the fraction corresponding to non-KT MTs) and the slow (typically interpreted as the fraction corresponding KT MTs) processes were obtained. The half-life was calculated as ln2/k for each MT population.

Determination of the frequency of lagging chromosomes forming a micronuclei

The frequency of lagging chromosomes forming micronuclei was determined considering only cells that had 1 or 2 lagging chromosomes in anaphase. Cells with > 2 lagging chromosomes were excluded to avoid overestimation. For cells with 1 or 2 lagging chromosomes in anaphase, the percentage of lagging chromosomes that resulted in micronuclei formation for each condition was calculated. Lagging chromosomes were tracked as cells exited mitosis. Only when chromosomes (lagging + segregating) decondensed, we assessed whether they formed micronuclei that were clearly not incorporated in the main nuclei, often several hours upon mitotic exit.

Quantification of mitotic errors

Mitotic errors were tracked and quantified manually through close inspection of H2B localization in single plane confocal images through the full z stack. Mitotic errors were divided into 2 main classes: lagging chromosomes or DNA bridges and these were discriminated according to location and morphology associated with H2B localization. Lagging chromosomes retained normal DNA condensation and emerged at different stages during anaphase. Most lagging chromosomes were of transient nature and were only scored if visibly delayed in relation to the main chromosome mass, for at least 2 min (i.e., 4 frames) during anaphase. DNA bridges were characterized by stretches of DNA that connected both daughter nuclei and often displayed aberrant DNA condensation as judged by H2B localization. For lagging chromosomes, DNA bridges and micronuclei, cells were classified as having 1, 2 or > 2 events. To determine micronuclei origin, fully formed micronuclei were backtracked to reveal whether these originated from unaligned chromosomes, lagging chromosomes or DNA bridges. Only micronuclei derived from lagging chromosomes were considered in this study.

Quantification of the Aurora B phosphorylation gradient (Front/Back and Lagging/Daughter ratio)

Quantification of the Aurora B gradient in anaphase was performed in both fixed and live cells using phosphorylation of histone H3 at Serine 10 (pH3) as a readout for Aurora B activity on chromosomes. For Front/Back pH3 gradient measurements, each daughter nuclei was divided into near-equal parts: one closer to the midzone (Front) and the other closer to the pole (Back). Background subtracted mean pixel intensities of these regions were measured using ImageJ software and ratios calculated by dividing the 'Front'

Mean Pixel Intensity / 'Back' Mean Pixel Intensity. For Lagging/Daughter pH3 gradient measurements, background subtracted mean pixel intensities for the lagging chromosome (Lagging) and a corresponding region on daughter nuclei (Daughter) were measured using ImageJ software and ratios calculated by dividing the 'Lagging' Mean Pixel Intensity / 'Daughter' Mean Pixel Intensity. Note that a ratio close to 1 indicates that there is no difference in pH3 levels throughout the DNA. Conversely, a ratio below 1 indicates that the levels of pH3 are lower on the DNA closer to the midzone.

Quantification of spindle elongation, chromosome separation velocity and chromosome separation distance

Spindle elongation velocities were measured from images displaying mCherry-α-tubulin. Centrosome to centrosome distance was measured at anaphase onset and at 3 min after anaphase onset and calculations represent the elongation rate (μm/min) for each spindle. Chromosome separation velocities were measured from images displaying H2B-GFP by calculating chromosome separation distance between 0-3 min after anaphase onset (corresponding to the time frame with the fastest linear elongation velocity). Chromosome separation distance was calculated by measuring the average distance between each chromosome mass (H2B) 7 min after anaphase onset. Measurements were performed using ImageJ software.

Quantification of pH3 and Nup153 in live cells

Quantifications were performed using sum projections of in-focus frames for each channel. For Figures 5E and 5F, the values for Nup153 and pH3 were normalized to the maximum (during the first 14 min of anaphase) and to the levels in metaphase, respectively. We considered a chromosome Nup153 positive when the amount of Nup153 recruited to lagging chromosomes was indistinguishable with the main nuclei.

Statistical Analysis

Quantifications of mitotic errors (i.e., lagging chromosomes, DNA bridges and micronuclei) were analyzed using the Fisher's exact two-tailed test. Quantification of NEB to anaphase duration was analyzed using the unpaired two-tailed test. Quantifications of chromosome separation velocity were analyzed using the Dunn's multiple comparisons test since not all conditions satisfied the Anderson-Darling, D'Agostino & Pearson, Shapiro-Wilk and Kolmogorov-Smirnov normality and log normality tests. Quantifications of spindle elongation, and chromosome segregation distance were analyzed using the Tukey's multiple comparisons test after confirming that all conditions satisfied the Anderson-Darling, D'Agostino & Pearson, Shapiro-Wilk and Kolmogorov-Smirnov normality and log normality tests. Quantification of the dynamics of Nup153 and LBR localization were analyzed using the Mann-Whitney test. Quantifications of pH3 Front/Back and Lagging/Daughter ratios were analyzed using the Mann-Whitney test. Quantifications of microtubule turnover in anaphase were analyzed using the Student's T Distribution test. Quantifications of dynamics of Aurora B were analyzed using a two-tailed t test. Quantifications of pPLK1 on lagging chromosomes versus polar chromosomes were analyzed using the Mann-Whitney test. For each graph, where applicable, n.d. = not determined, n.s. = non-significant, *$p \leq 0.05$, **$p \leq 0.01$ ***$p \leq 0.001$ and ****$p \leq 0.0001$, unless stated otherwise. Pearson Correlation Coefficient (PCC) was calculated using Excel CORREL function. All results presented in this manuscript were obtained from pooling data from at least 3 independent experiments with the exception of the results presented for depletions of KT proteins in HeLa cells in which 2 independent experiments were performed.